Electronic Supplementary Material (ESI) for Dalton Transactions.
This journal is © The Royal Society of Chemistry 2023

Electronic Supplementary Information for:

Impact of Ligand Chlorination and Counterion Tuning on High-Field Spin Relaxation in a Series of V(IV) Complexes

Roxanna Martinez,[1] Cassidy E. Jackson,[1] Ökten Üngör,[1] Johan van Tol,[2] and Joseph M. Zadrozny*[1]

[1]*Department of Chemistry, Colorado State University, Fort Collins, Colorado 80523, USA.*
[2]*National High Magnetic Field Laboratory, Tallahassee, Florida 32310, USA.*

Table of Contents

Full Experimental Details

Table S1. Crystallographic information for the structural refinement of **2**.

Empirical formula[a]	$H_{64}C_{42}N_2Cl_3O_6V \bullet 1.6[C_4H_8O]$
Formula weight	997.15
Temperature	110(2)
Crystal system	monoclinic
Space group	P 1 21/c 1
a	20.0922(9) Å
b	15.2744(8) Å
c	17.8164(9) Å
α	90°
β	105.925°
γ	90°
Volume	5257.9(5) $Å^3$
Z	4
ρ_{calc}	1.448 g/cm^3
μ	2.921 mm^{-1}
F(000)	2120
Crystal color	Dark blue
Crystal size	0.184 × 0.164 × 0.158 mm^3
Radiation	MoKα (λ = 0.71073 Å)
2θ range for data collection	1.699 to 28.268°
Index ranges	$-26 \leq h \leq 26$, $-20 \leq k \leq 20$, $-23 \leq l \leq 23$
Reflections collected	335992
Independent collections	13015 [R_{int} = 0.0666, R_{sigma} = 0.0179]
Data/restraints/parameters	13015/0/542
Goodness-of-fit on F^2	1.041
Final R indexes [I ≥ 2σ (I)]	R_1 = 0.065979, wR_2 = 0.2051
Final R indexes [all data]	R_1 = 0.082232, wR_2 = 0.2306
Largest diff. peak/hole	0.98/–0.52 e $Å^{-3}$
Flack parameter	0.000(4)

[a]Solvent mask used for stoichiometric details: see CIF and experimental section for details.

Table S2. Crystallographic information for the structural refinement of **5**.

Empirical formula[a]	$H_{62}C_{42}N_2Cl_6O_6V \bullet 1.7[C_4H_8O]$
Formula weight	954.57
Temperature	104(2)
Crystal system	trigonal
Space group	P31 2 1
a	15.2509(4) Å
b	15.2509(4) Å
c	18.9173(6) Å
α	90°
β	90°
γ	120°
Volume	3810.5(2) $Å^3$
Z	3
ρ_{calc}	1.248 g/cm^3
μ	0.553 mm^{-1}
F(000)	1503
Crystal color	Dark blue
Crystal size	$0.143 \times 0.117 \times 0.0181$ mm^3
Radiation	MoKα (λ = 0.71073 Å)
2θ range for data collection	1.542 to 27.472°
Index ranges	$-19 \leq h \leq 19$, $-19 \leq k \leq 19$, $-24 \leq l \leq 24$
Reflections collected	227182
Independent collections	5840 [R_{int} = 0.0832, R_{sigma} = 0.0181]
Data/restraints/parameters	5840/0/261
Goodness-of-fit on F^2	1.120
Final R indexes [$I \geq 2\sigma$ (I)]	R_1 = 0.0304, wR_2 = 0.0794
Final R indexes [all data]	R_1 = 0.0362, wR_2 = 0.0892
Largest diff. peak/hole	0.95/–0.69 e $Å^{-3}$
Flack parameter	0.0(7)

[a]Solvent mask used for stoichiometric details see CIF file and experimental section

Table S3. Crystallographic information for the structural refinement of **6**.

Empirical formula	$C_{42}H_{56}Cl_{12}N_2O_6V$
Formula weight	1161.22
Temperature	99.9(7)
Crystal system	triclinic
Space group	P-1
a	11.541(10) Å
b	12.302(10) Å
c	37.11(2) Å
α	95.54(10)°
β	106.49(10)°
γ	95.79(10)°
Volume	2575.27(4) $Å^3$
Z	2
ρ_{calc}	2.048 g/cm^3
μ	7.717 mm^{-1}
F(000)	1194
Crystal color	Dark blue
Crystal size	0.126 x 0.074 x 0.054 mm^3
Radiation	MoKα (λ = 0.71076 Å)
2θ range for data collection	2.424 to 78.171°
Index ranges	$-14 \leq h \leq 15$, $-15 \leq k \leq 15$, $-24 \leq l \leq 24$
Reflections collected	60728
Independent collections	10949 [R_{int} = 0.0422, R_{sigma} = 0.0332]
Data/restraints/parameters	10949 /876/690
Goodness-of-fit on F^2	1.078
Final R indexes [$I \geq 2\sigma$ (I)]	R_1 = 0.0441, wR_2 = 0.1087
Final R indexes [all data]	R_1 = 0.0487, wR_2 = 0.1123
Largest diff. peak/hole	1.24/–1.54 e $Å^{-3}$
Flack parameter	0.065(5)

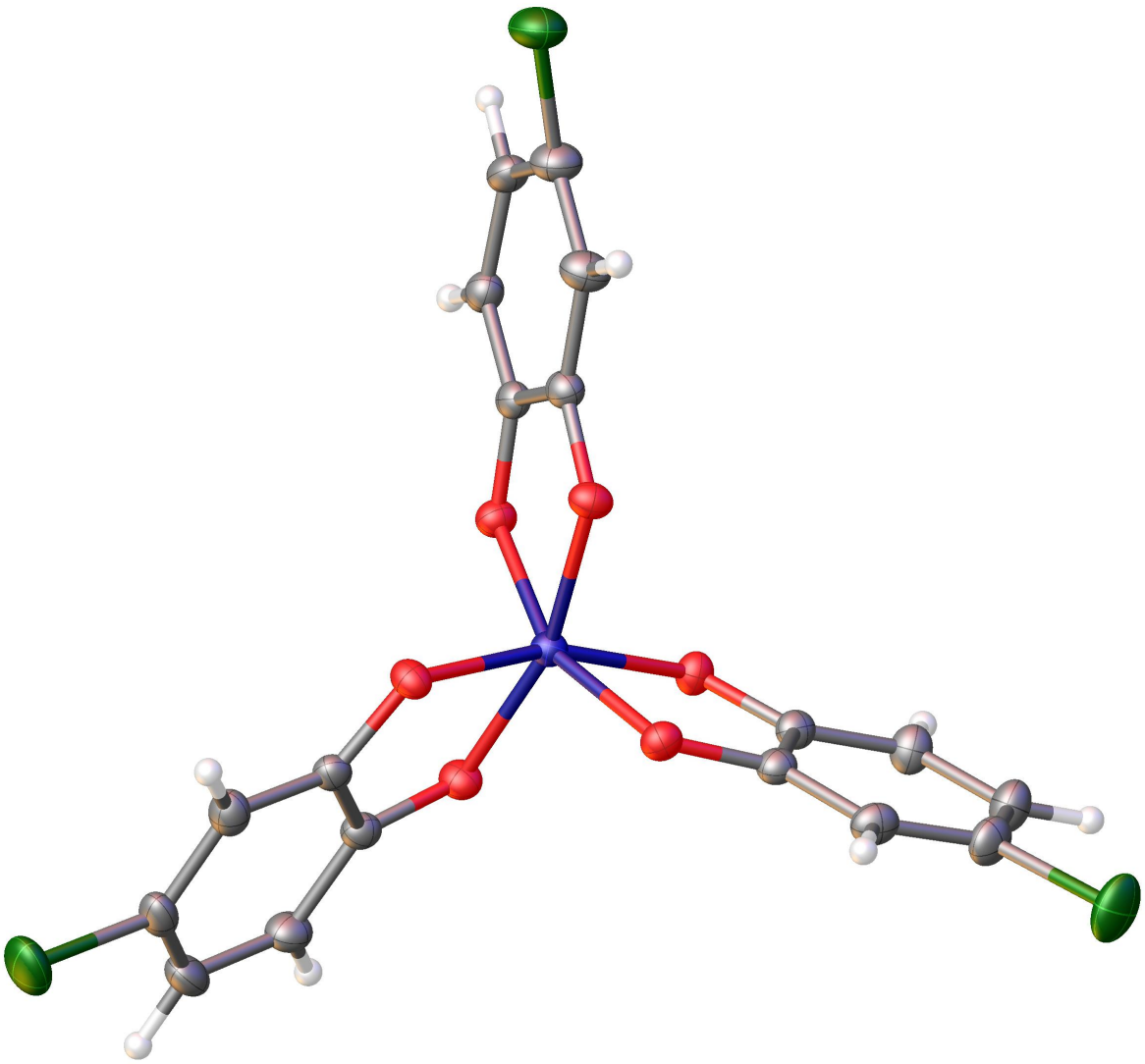

Figure S1. Thermal ellipsoid plot of **2** drawn at the 50% probability level. Counterions and solvent molecules were removed for clarity. Purple, red, green, grey, and white ellipsoids correspond to vanadium, oxygen, chlorine, carbon, and hydrogen, respectively.

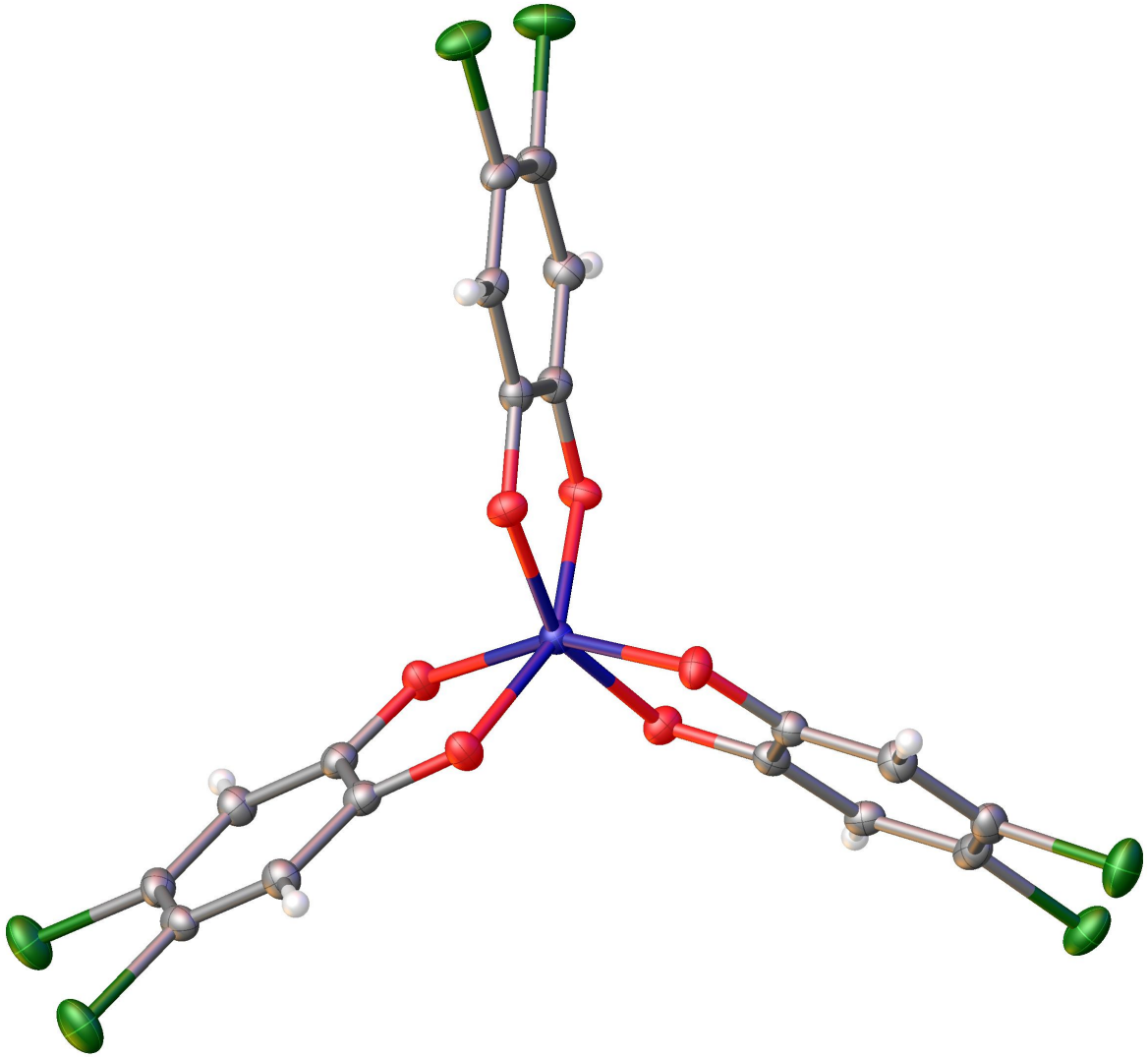

Figure S2. Thermal ellipsoid plot of **5** drawn at the 50% probability level. Counterions and solvent molecules were removed for clarity. Purple, red, green, grey, and white ellipsoids correspond to vanadium, oxygen, chlorine, carbon, and hydrogen, respectively.

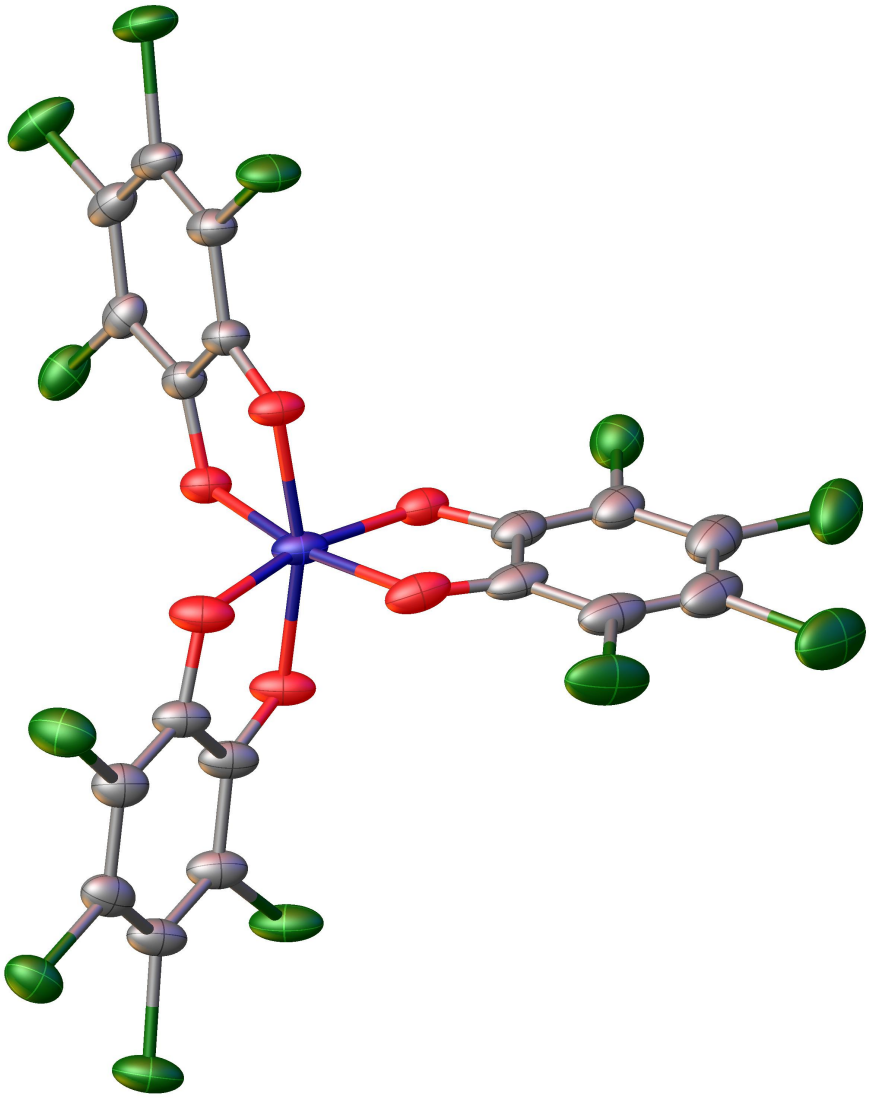

Figure S3. Thermal ellipsoid plot of **6** drawn at the 50% probability level. Counterions and solvent molecules were removed for clarity. Purple, red, green, grey, and white ellipsoids correspond to vanadium, oxygen, chlorine, carbon, and hydrogen, respectively.

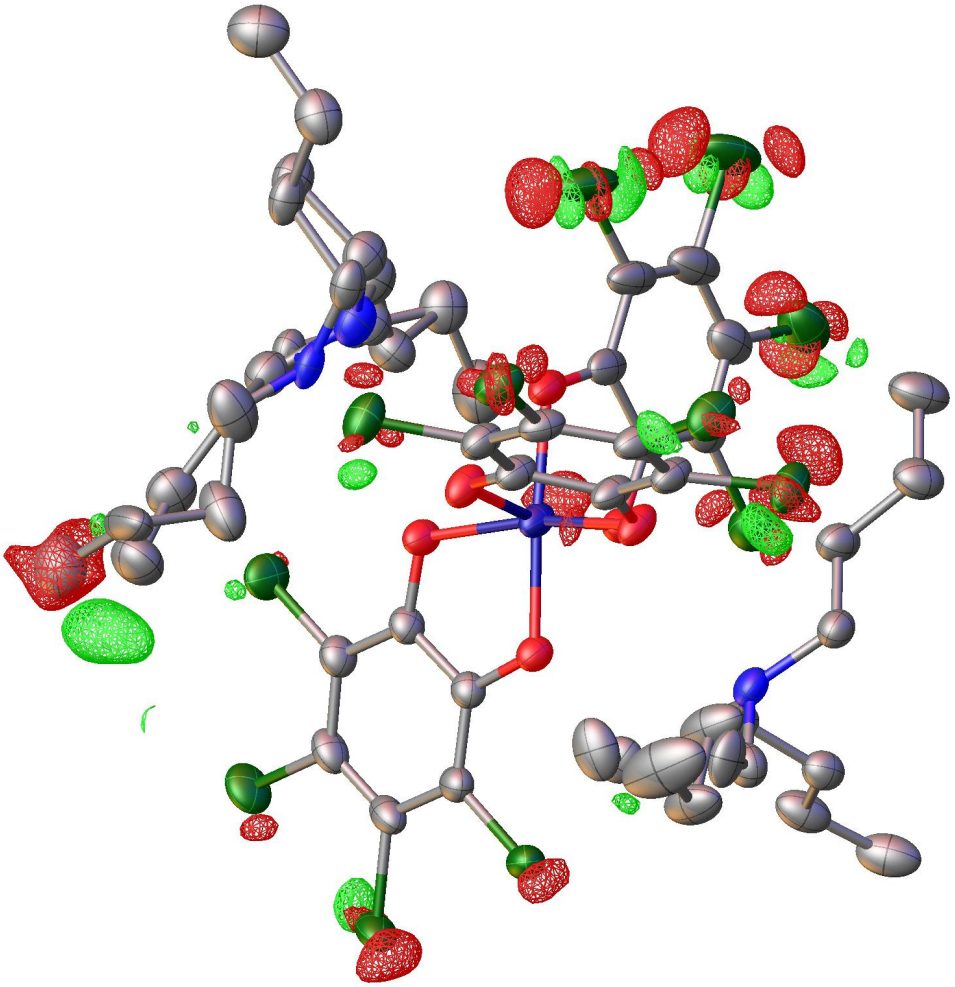

Figure S4. Electron density map of **6** suggesting slight unresolved disorder on the ligands and counterions. Residual electron density in the unit cell is located primarily near the Cl atoms and extends along the longest anisotropic displacement axes, which is common for heavy atoms and suggests slight ligand disorder. Hydrogens were omitted for clarity. Purple, red, green, grey, and white ellipsoids correspond to vanadium, oxygen, chlorine, and carbon, respectively.

Table S4. Calculated Bailar twist angle (θ) for complexes **1-6.**

Complex	θ_1	θ_2	θ_3	Avg. θ
(n-$Bu_3NH)_2[V(C_6\mathbf{H_4}O_2)_3]$	27.33	27.33	25.22	26.62
(n-$Bu_3NH)_2[V(\mathbf{4\text{-}Br}\text{-}C_6H_3O_2)_3]$	23.34	27.47	23.34	24.71
(n-$Bu_3NH)_2[V(\mathbf{4,5\text{-}Br_2}\text{-}C_6H_3O_2)_3]$	18.93	18.00	18.93	18.62
(n-$Bu_3NH)_2[V(C_6\mathbf{Br_4}O_2)_3]$	28.08	33.82	26.98	29.63
(n-$Bu_3NH)_2[V(\mathbf{4\text{-}Cl}\text{-}C_6H_3O_2)_3]$	23.34	22.76	24.93	23.35
(n-$Bu_3NH)_2[V(\mathbf{4,5\text{-}Cl_2}\text{-}C_6H_3O_2)_3]$	18.70	18.63	18.70	18.67
(n-$Bu_3NH)_2[V(C_6\mathbf{Cl_4}O_2)_3]$	26.52	31.78	26.94	28.41

Table S5. EDFS spin Hamiltonian parameters for **1**–**8** in d^{14}-*o*-terphenyl collected at 5 K. The standard errors for these parameters were not available from the simulating process.

Complex	**1**	**2**	**3**	**4**	**5**	**6**	**7**	**8**
g_x	1.939	1.943	1.942	1.940	1.942	1.938	1.940	1.940
g_y	1.923	1.923	1.925	1.920	1.915	1.913	1.920	1.918
g_z	1.990	1.992	1.993	1.993	1.993	1.992	1.991	1.990
g_x strain	0.0042	0.0045	0.0045	0.0045	0.0052	0.0042	0.0045	0.0045
g_y strain	0.0129	0.028	0.028	0.028	0.020	0.019	0.028	0.028
g_z strain	0	0	0	0	0	0	0	0
A_x (MHz)	301	245	270	295	285	275	280	298
A_y (MHz)	348	385	365	365	360	350	350	350
A_z (MHz)	53	60	60	50	50	70	50	50

*Changes in *A*-strain resulted in no change in the simulated spectrum.

Table S6. Spin Hamiltonian parameters for **1**-**6** in toluene collected at 100 K by CW X-band EPR. The standard errors for these parameters were not available from the simulating process.

Complex	**1**	**2**	**3**	**4**	**5**	**6**
g_x	1.940	1.928	1.935	1.928	1.932	1.928
g_y	1.932	1.935	1.932	1.925	1.925	1.925
g_z	1.992	1.990	1.985	1.981	1.983	1.980
A_x (MHz)	290	300	285	285	285	290
A_y (MHz)	345	345	365	363	363	370
A_z (MHz)	55	60	60	60	60	65
LWPP	4	4	4	4	4	4

Table S7. Spin Hamiltonian parameters for **2**-**6** in toluene collected at 298 K by CW X-band EPR. The standard errors for these parameters were not available from the simulating process.

Complex	**2**	**3**	**4**	**5**	**6**
g_x	1.923	1.925	1.930	1.920	1.920
g_y	1.940	1.940	1.935	1.940	1.942
g_z	1.991	1.986	1.981	1.982	1.990
A_x (MHz)	300	305	300	305	310
A_y (MHz)	350	355	350	350	350
A_z (MHz)	60	60	60	60	60
τ_{corr} (ps)	402	420	418	415	427

Table S8. Fit T_1 values from the fitting function: $I(\tau) = I(0) - Ae^{-\left(\frac{\tau}{T_1}\right)^{\beta}}$. The standard error for each fit is reported in parentheses.

1 in d^{14}-*o*-terphenyl:

T (K)	T_1 (ms)	T (K)	T_1 (ms)
4	1.23(6)	15	0.26(1)
5	1.15(3)	20	0.09(1)
10	0.43(1)		

2 in d^{14}-*o*-terphenyl:

T (K)	T_1 (ms)	T (K)	T_1 (ms)
5	0.24(2)	15	0.12(1)
10	0.23(5)	20	0.079(2)
12	0.17(6)		

3 in d^{14}-*o*-terphenyl:

T (K)	T_1 (ms)	T (K)	T_1 (ms)
5	0.59(1)	15	0.14(7)
10	0.24(3)	20	0.09(5)
12	0.20(7)		

4 in d^{14}-*o*-terphenyl:

T (K)	T_1 (ms)	T (K)	T_1 (ms)
5	0.63(1)	15	0.13(2)
10	0.65(2)	20	0.08(5)
12	0.26(1)		

5 in d^{14}-*o*-terphenyl:

T (K)	T_1 (ms)	T (K)	T_1 (ms)
5	0.56(4)	15	0.14(2)
10	0.30(2)	20	0.09(2)
12	0.21(3)		

6 in d^{14}-*o*-terphenyl:

T (K)	T_1 (ms)	T (K)	T_1 (ms)
5	0.46(4)	15	0.13(3)
10	0.37(5)	20	0.08(3)
12	0.18(2)		

7 in d^{14}-*o*-terphenyl:

T (K)	T_1 (ms)	T (K)	T_1 (ms)
5	0.57(6)	15	0.15(3)
10	0.22(4)		
12	0.19(2)		

8 in d^{14}-*o*-terphenyl:

T (K)	T_1 (ms)	T (K)	T_1 (ms)
5	1.55(2)	15	0.32(3)
10	1.08(5)	20	0.12(3)
12	0.62(4)		

Table S9. Fit parameters for the temperature dependence of T_1; see "EPR measurements" section for fitting equation. The standard error for each fit is reported in parentheses.

Complex	A_{dir} (K^{-1} s^{-1} T^{-2})	A_{ram}(s^{-1})
1	$6.01(3)\times10^{-4}$	$4.76(5)\times10^{-12}$
2	$1.36(1)\times10^{-3}$	$9.18(6)\times10^{-12}$
3	$1.13(4)\times10^{-3}$	$7.57(2)\times10^{-12}$
4	$9.98(2)\times10^{-4}$	$2.37(2)\times10^{-11}$
5	$1.10(4)\times10^{-3}$	$1.93(3)\times10^{-11}$
6	$1.13(1)\times10^{-3}$	$1.78(8)\times10^{-11}$

*Values for B and n were fixed.

Table S10. Fit T_m values (in μs) and the stretch parameters (β) from the stretched exponential fitting function: $I(2\tau) = I(0) - Ae^{(\frac{2\tau}{T_m})^{\beta}}$. The standard error for each fit is reported in parentheses.

1 in d^{14}-*o*-terphenyl:

T (K)	T_m (μs)	β	T(K)	T_m (μs)	β
4	5.44(2)	0.66(2)	15	2.81(4)	0.80(1)
5	4.82(3)	0.68(3)	20	2.45(4)	0.86(2)
6	4.56(2)	0.70(3)	25	2.14(4)	0.91(2)
8	3.92(3)	0.74(4)	30	1.86(3)	0.94(2)
10	3.39(3)	0.77(6)			

2 in d^{14}-*o*-terphenyl:

T (K)	T_m (μs)	β	T(K)	T_m (μs)	β
5	3.91(7)	0.64(8)	20	2.07(2)	0.83(1)
6	3.67(4)	0.68(5)	25	1.89(2)	0.86(1)
8	3.25(3)	0.72(5)	30	1.71(2)	0.87(1)
12	2.82(4)	0.73(1)	40	1.41(3)	0.92(2)
15	2.31(6)	0.92(3)	60	0.74(7)	0.77(7)

3 in d^{14}-*o*-terphenyl:

T (K)	T_m (μs)	β	T(K)	T_m (μs)	β
5	4.54(6)	0.66(1)	15	2.78(1)	0.72(3)
7	4.01(7)	0.68(1)	20	2.37(9)	0.76(3)
8	3.74(9)	0.70(2)	25	2.07(8)	1.05(6)
10	3.23(6)	0.69(1)	30	2.41(9)	1.30(1)
12	3.03(6)	0.70(1)			

4 in d^{14}-*o*-terphenyl:

T (K)	T_m (μs)	β	T(K)	T_m (μs)	β
5	4.33(4)	0.63(5)	15	2.53(4)	0.72(1)
7	3.88(4)	0.67(5)	20	2.27(4)	0.75(2)
8	3.69(4)	0.68(6)	25	2.01(4)	0.78(2)
10	3.13(4)	0.71(8)	30	2.06(5)	0.83(3)
12	2.85(5)	0.72(1)	40	1.73(6)	0.74(2)

5 in d^{14}-*o*-terphenyl:

T (K)	T_m (μs)	β	T(K)	T_m (μs)	β
5	4.17(2)	0.68(3)	20	2.11(1)	0.82(6)
7	3.57(2)	0.70(4)	25	1.85(1)	0.85(6)
8	3.61(2)	0.88(5)	30	1.72(2)	0.91(7)
10	2.95(1)	0.74(4)	40	1.44(3)	0.96(1)
12	2.67(1)	0.77(5)	50	1.14(1)	0.99(1)
15	2.36(3)	0.80(7)			

6 in d^{14}-*o*-terphenyl:

T (K)	T_m (μs)	β	T(K)	T_m (μs)	β
5	3.84(3)	0.64(4)	20	2.19(2)	0.78(8)
7	3.50(2)	0.66(4)	25	1.97(2)	0.79(1)
8	3.42(6)	0.67(1)	30	1.83(3)	0.77(1)
10	3.07(3)	0.70(5)	40	1.52(3)	0.79(2)
12	2.67(2)	0.72(5)			
15	2.47(2)	0.76(6)			

7 in d^{14}-*o*-terphenyl:

T (K)	T_m (μs)	β	T(K)	T_m (μs)	β
5	3.62(4)	0.64(3)	20	1.72(8)	1.00(3)
8	3.00(2)	0.74(8)	25	1.61(6)	1.02(4)
10	2.70(1)	0.82(1)	30	1.46(4)	1.05(4)
12	2.28(5)	0.84(2)			
15	2.07(5)	0.92(4)			

8 in d^{14}-*o*-terphenyl:

T (K)	T_m (μs)	β	T(K)	T_m (μs)	β
5	4.04(6)	1.08(2)	20	1.93(2)	1.09(1)
8	3.32(8)	1.08(3)			
10	2.91(9)	1.09(4)			
12	2.65(9)	1.10(5)			
15	2.30(1)	1.09(6)			

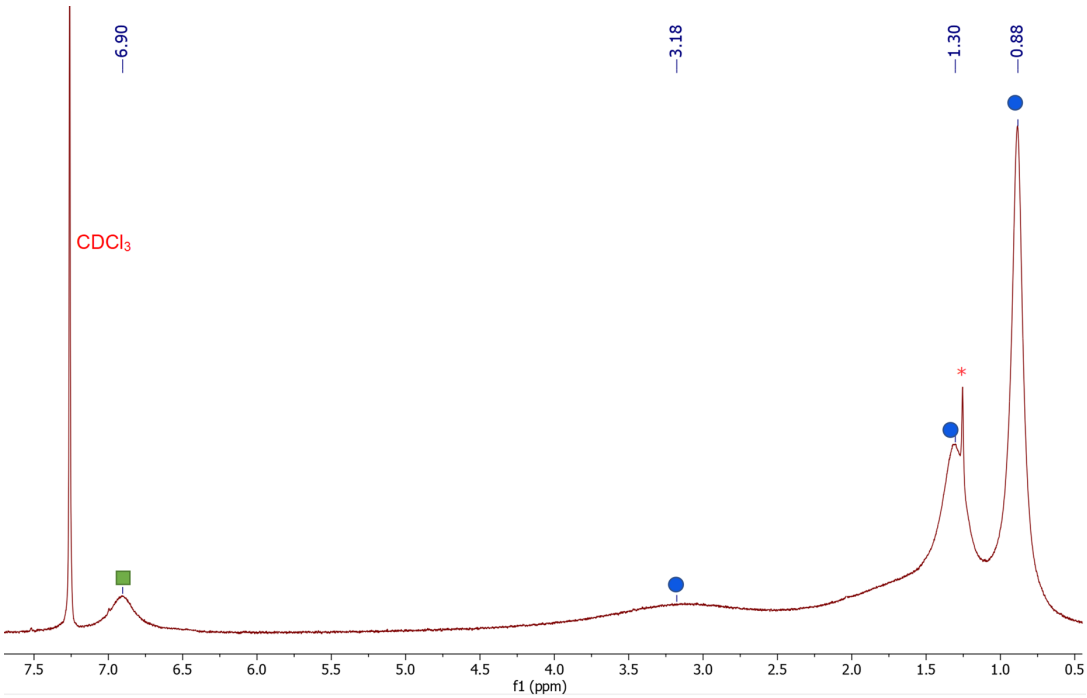

Figure S5. ^{1}H NMR spectrum of **2** in $CDCl_3$. No signal was observed outside this spectral range. Blue dots denote protons on the counterion, and the green square denote ligand protons. Asterisks denote impurities in the NMR solvent.

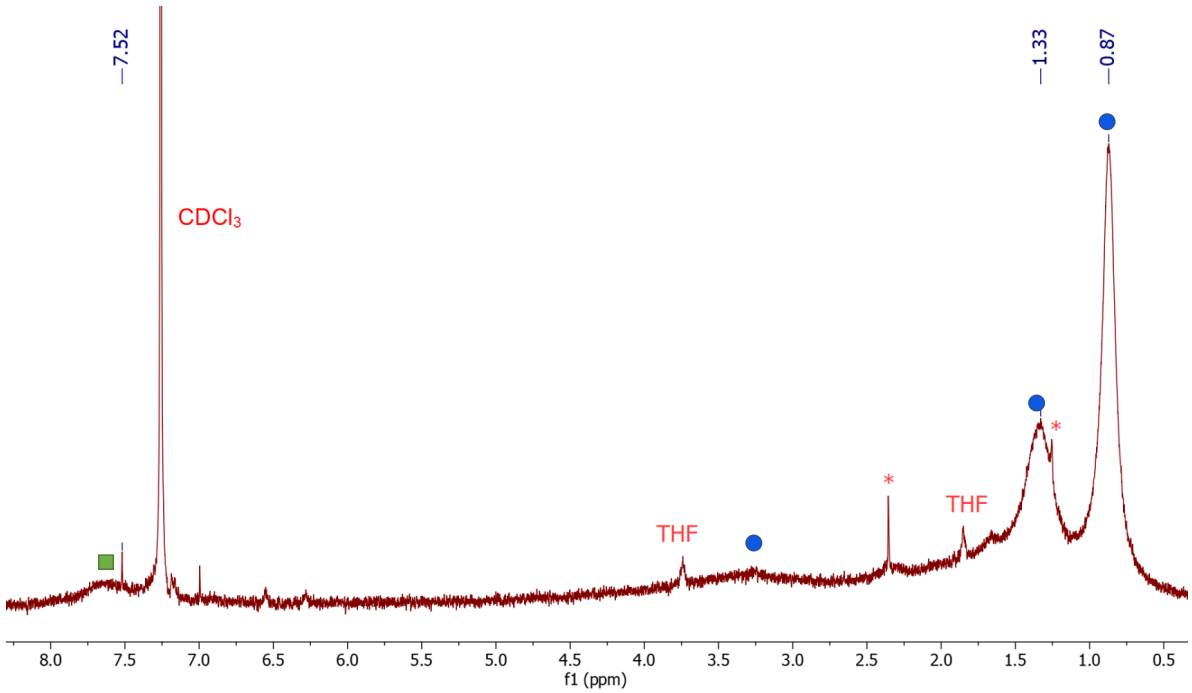

Figure S6. ^{1}H NMR spectrum of **3** in $CDCl_3$. No signal was observed outside this spectral range. Blue dots denote protons on the counterion, and the green square denote ligand protons. Asterisks denote impurities in the NMR solvent.

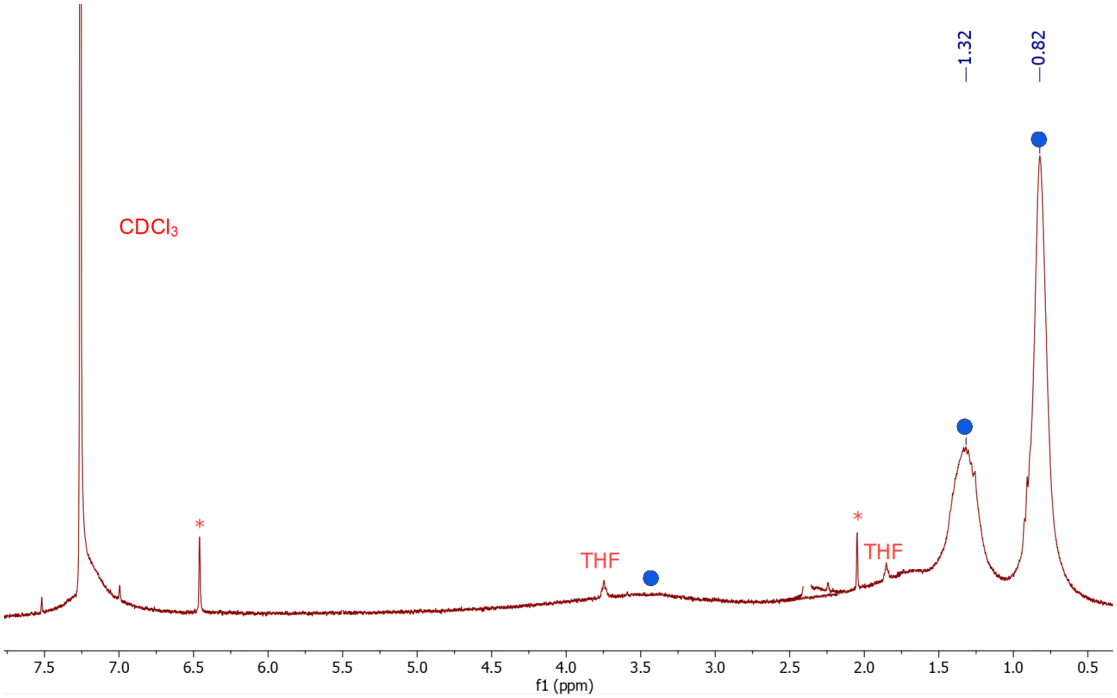

Figure S7. ^{1}H NMR spectrum of **4** in $CDCl_3$. No signal was observed outside this spectral range. Blue dots denote protons on the counterion. Asterisks denote impurities in the NMR solvent.

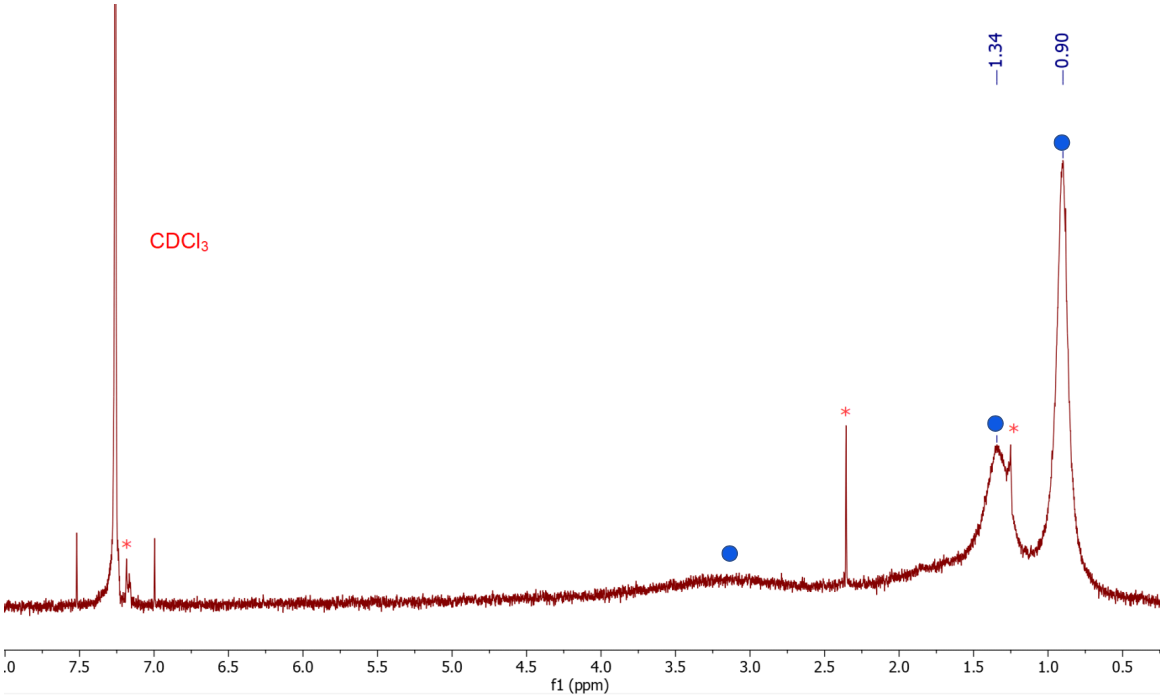

Figure S8. ^{1}H NMR spectrum of **5** in $CDCl_3$. No signal was observed outside this spectral range. Blue dots denote protons on the counterion. Asterisks denote impurities in the NMR solvent.

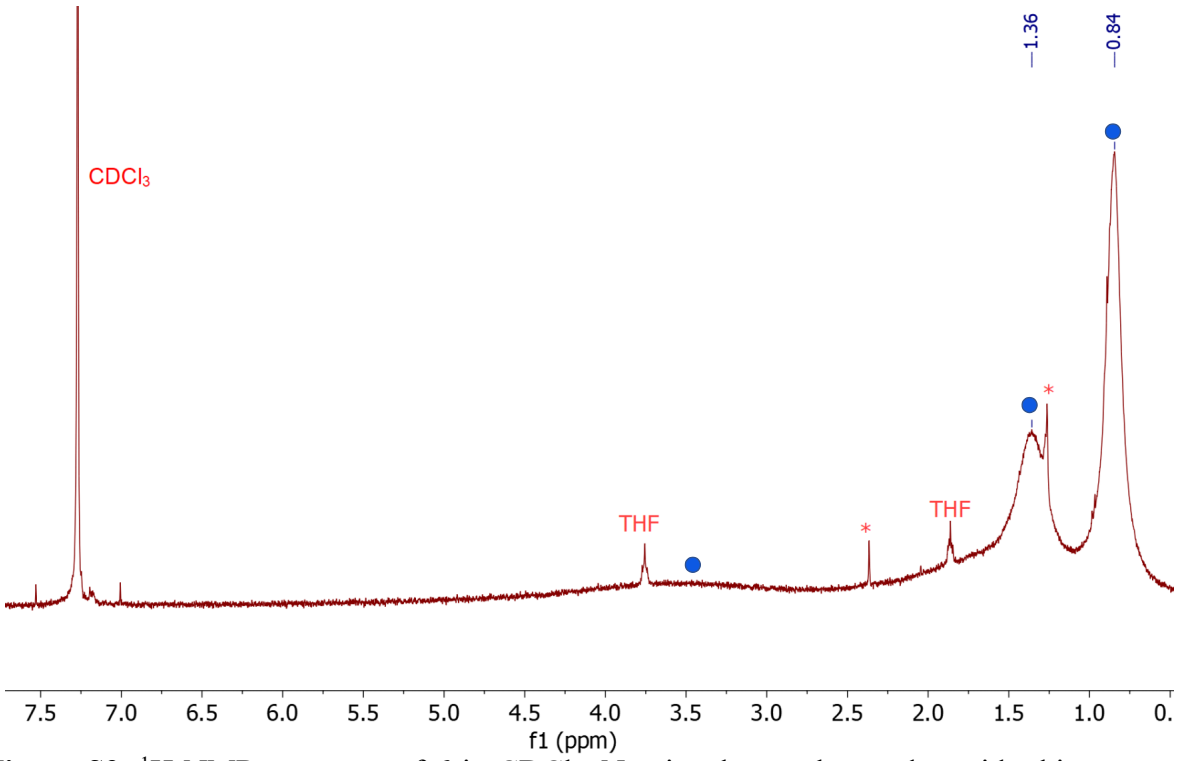

Figure S9. ^{1}H NMR spectrum of **6** in $CDCl_3$. No signal was observed outside this spectral range. Blue dots denote protons on counterion. Asterisks denote impurities in the NMR solvent.

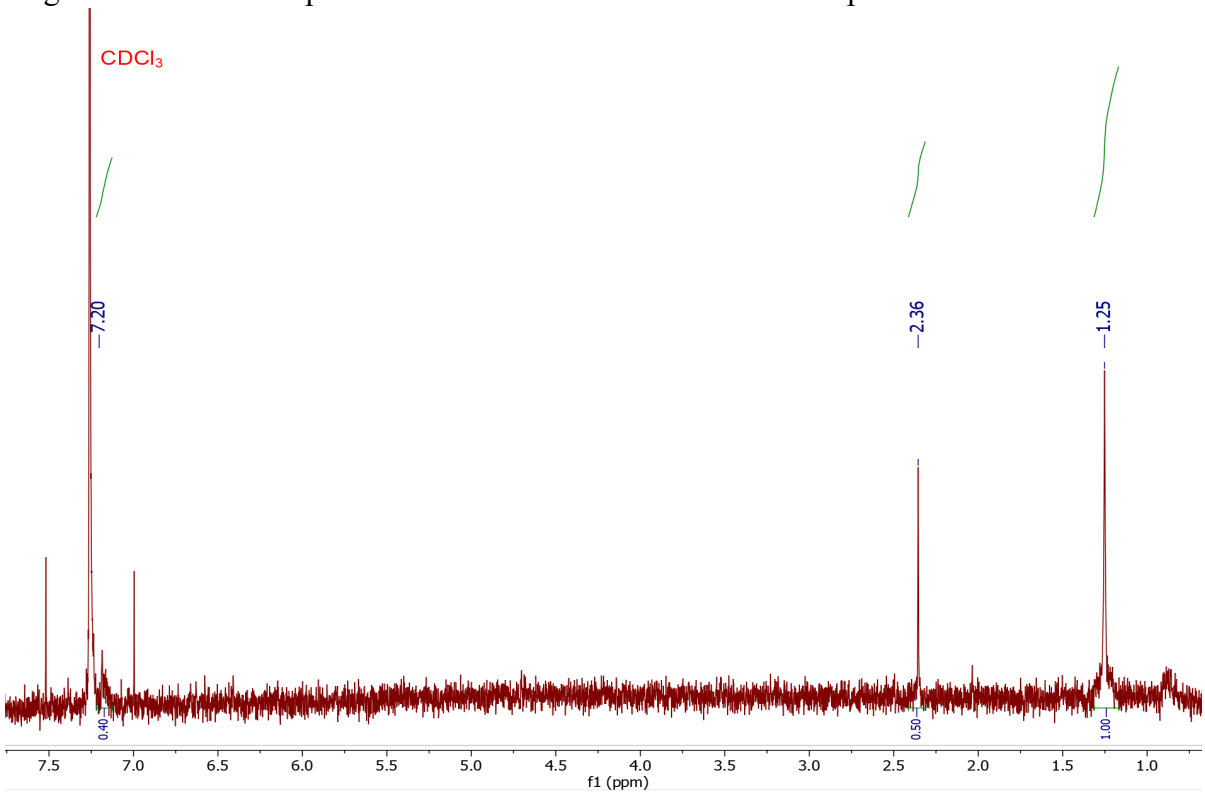

Figure S10. ^{1}H NMR spectrum of $CDCl_3$ used for collecting ^{1}H NMR spectra of complexes No signal was observed outside this spectral range. Numbered peaks correspond to solvent impurities.

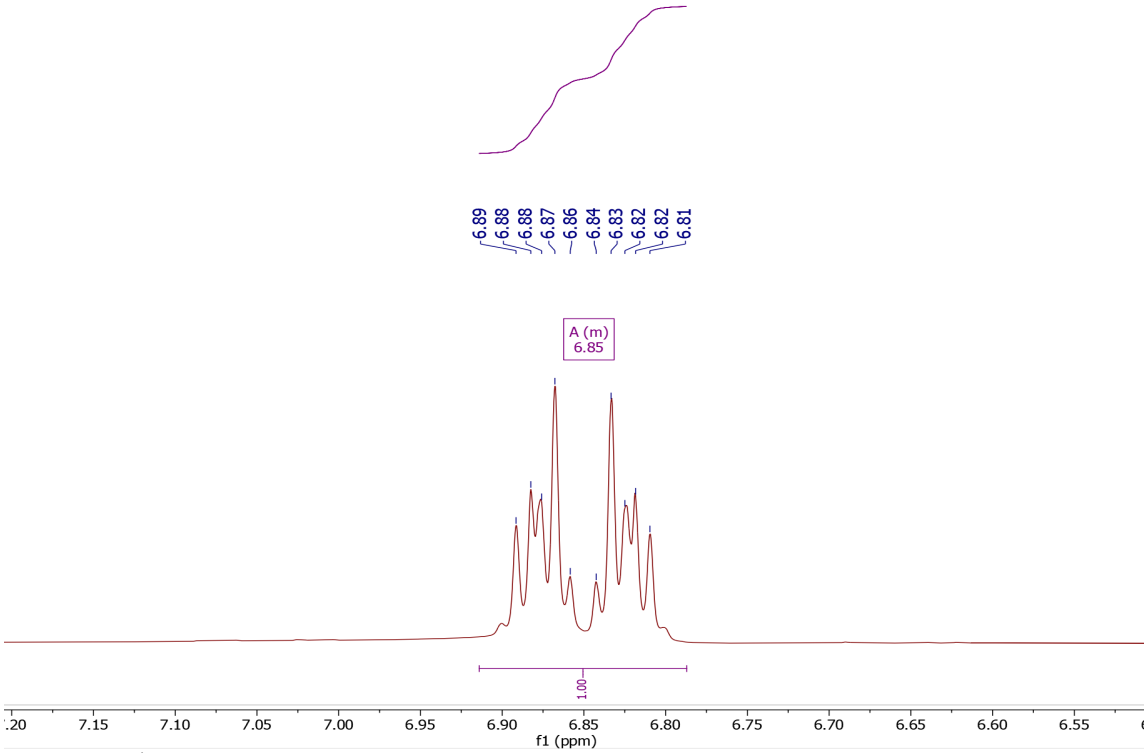

Figure S11. ^{1}H NMR spectrum of catechol ligand in $CDCl_3$. No signal was observed outside this spectral range.

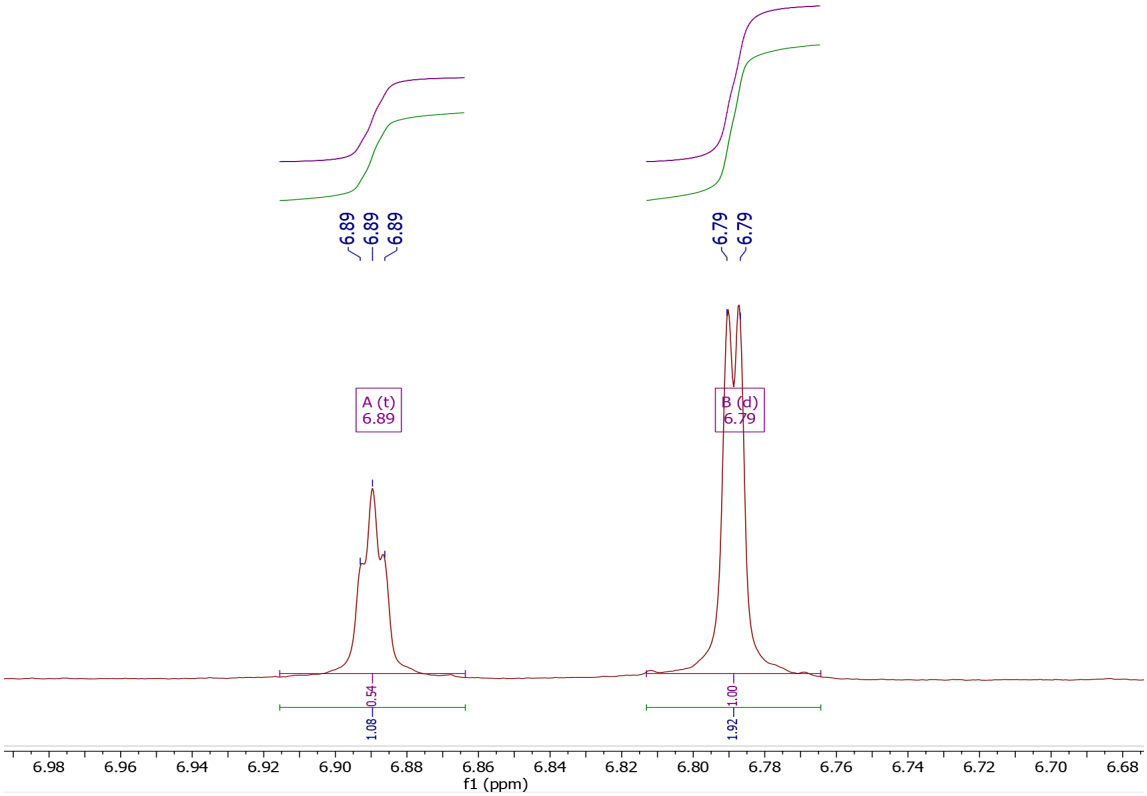

Figure S12. ^{1}H NMR spectrum of 4-chlorocatechol ligand in $CDCl_3$. No signal was observed outside this spectral range.

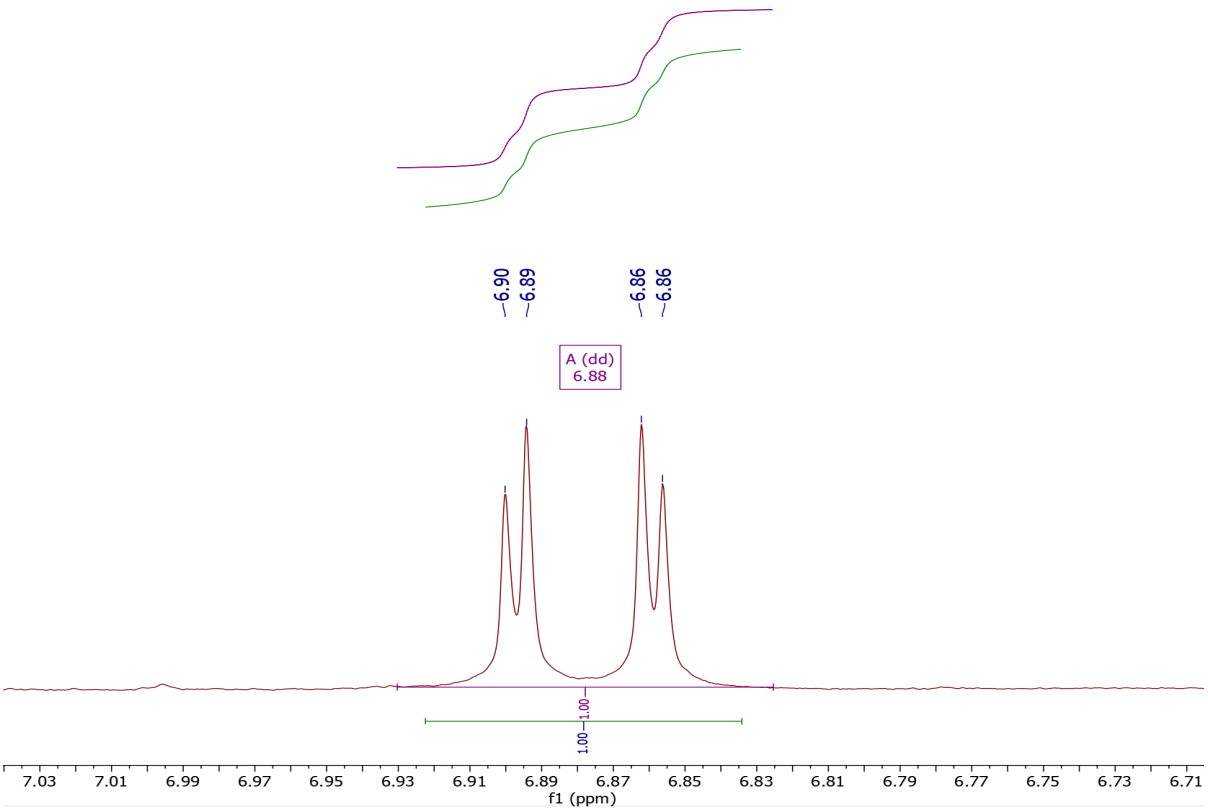

Figure S13. ^{1}H NMR spectrum of 3,5-dichlorocatechol ligand in $CDCl_3$. No signal was observed outside this spectral range.

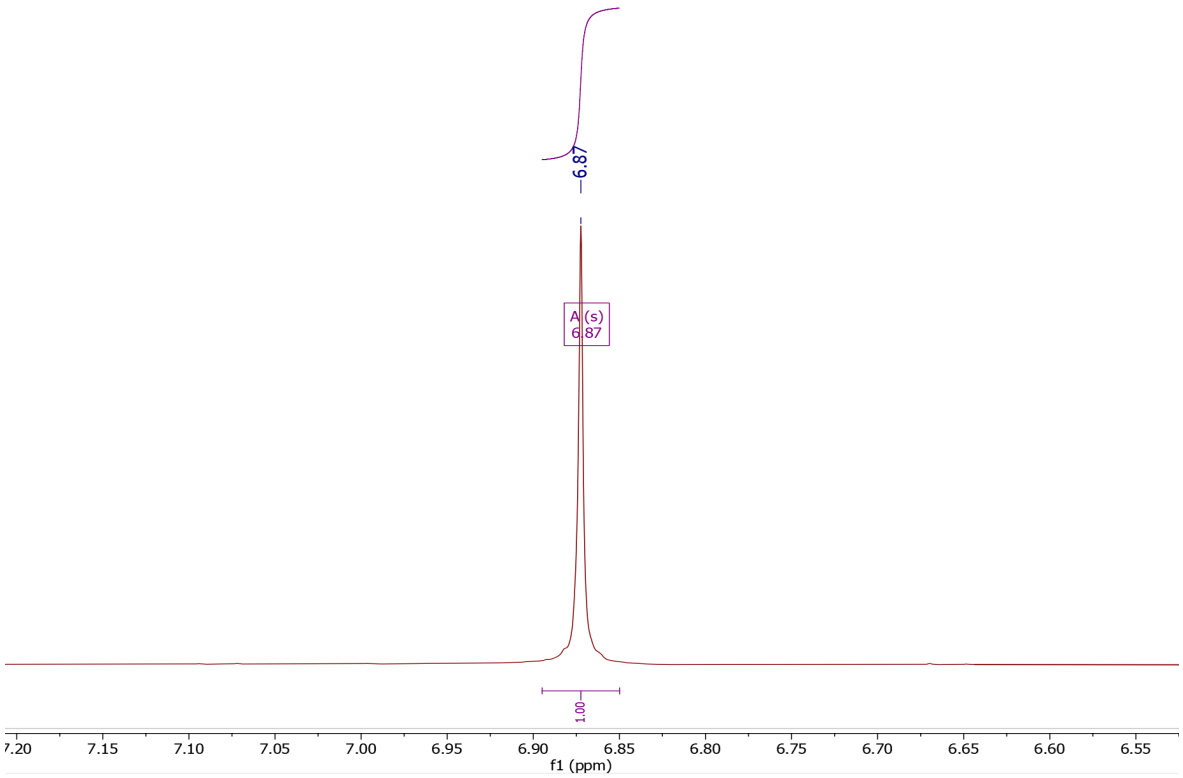

Figure S14. ^{1}H NMR spectrum of 3,6-dichlorocatechol ligand in $CDCl_3$. No signal was observed outside this spectral range.

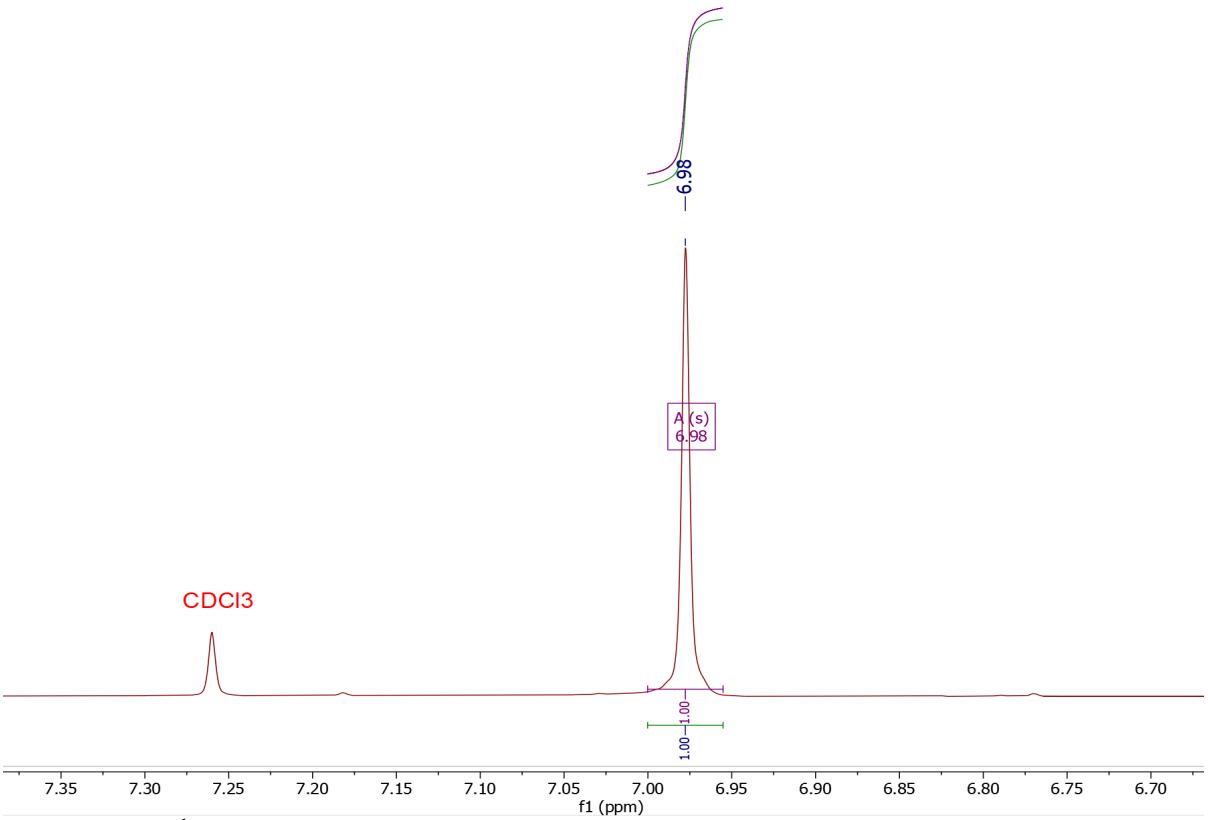

Figure S15. ^{1}H NMR spectrum of 4,5-dichlorocatechol ligand in $CDCl_3$. No signal was observed outside this spectral range.

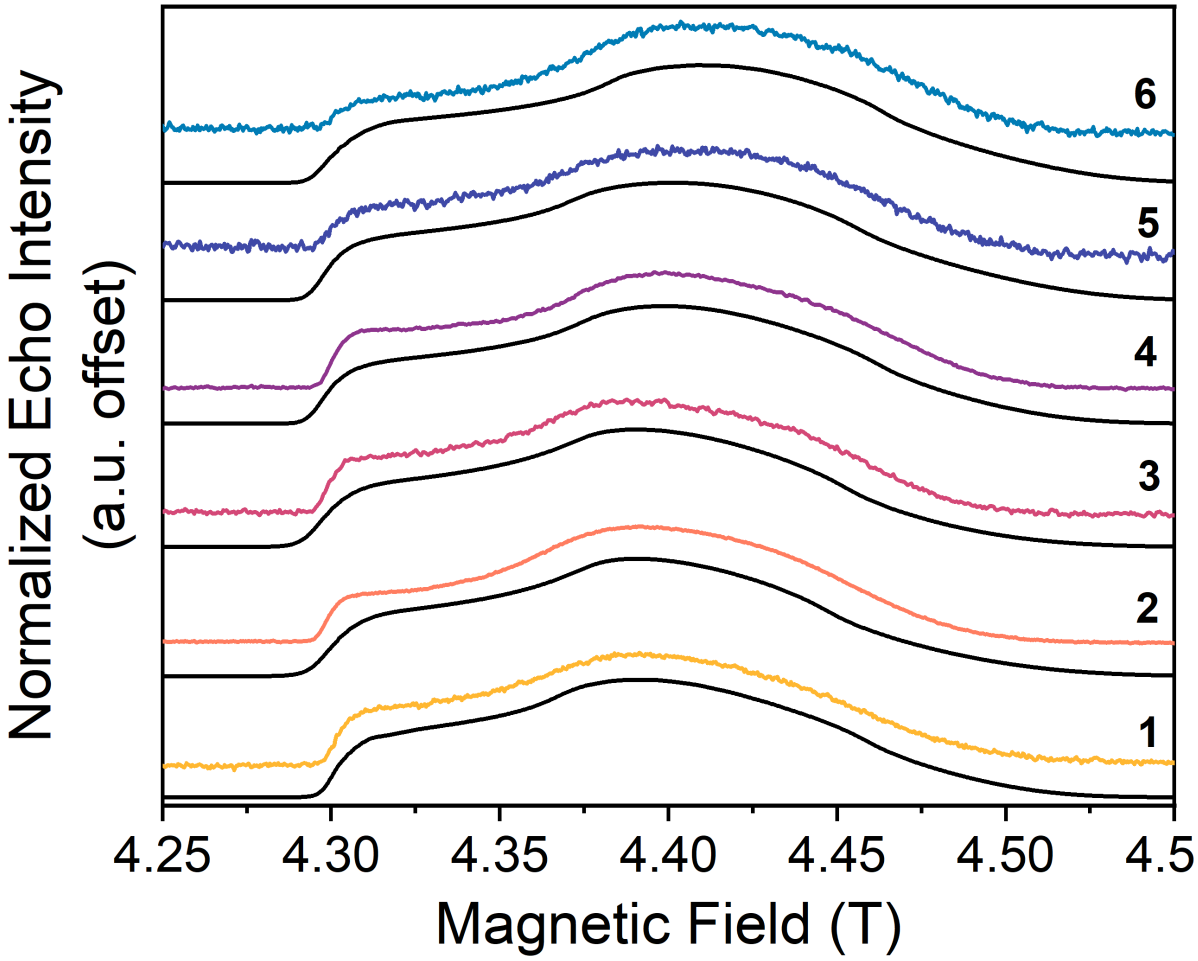

Figure S16. Echo-detected, field-swept spectra at 120 GHz of **1**–**6** in d^{14}–*o*–terphenyl solutions (color) at 5 K and simulations (black). Simulated spin Hamiltonian parameters are given in Table S4.

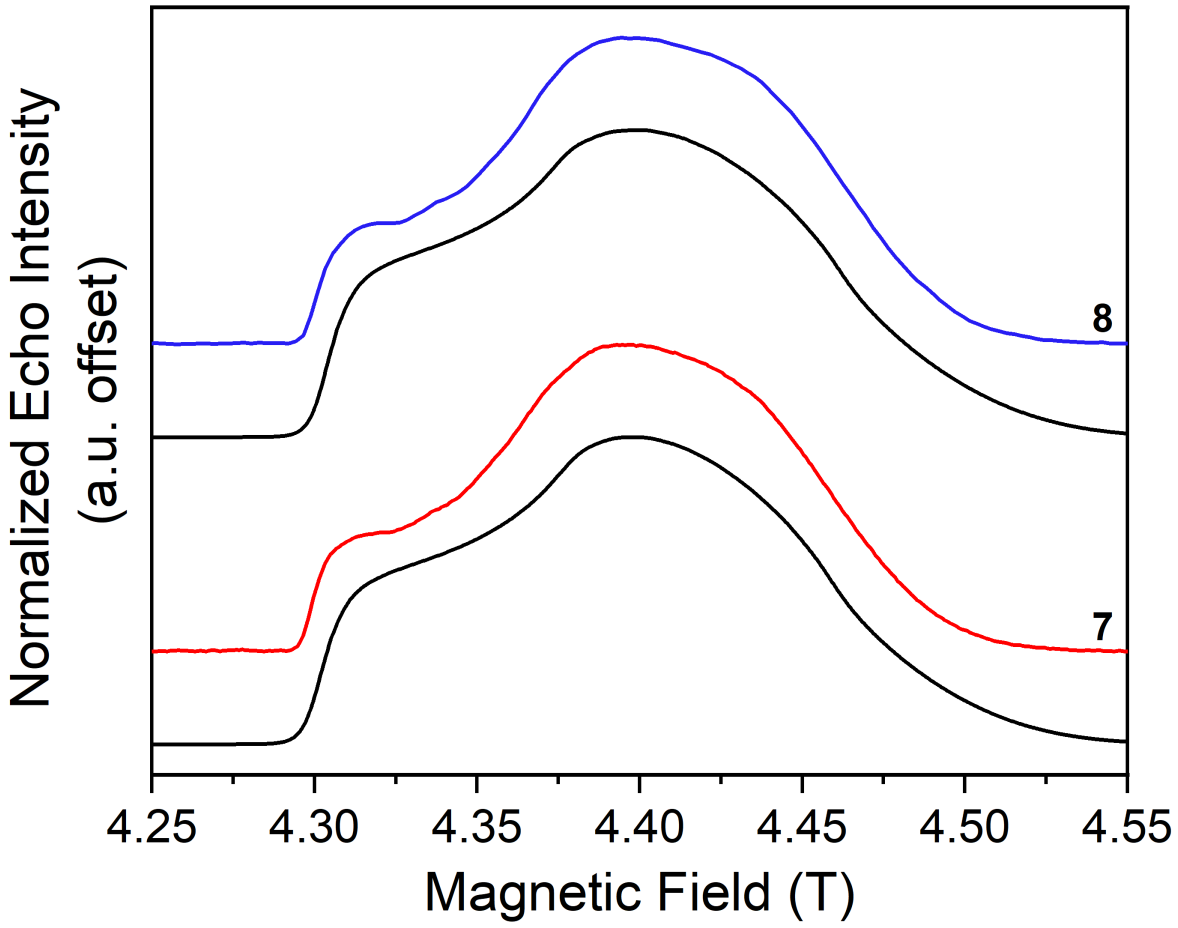

Figure S17. Echo-detected, field-swept spectra at 120 GHz of **7** and **8** in d^{14}–*o*–terphenyl solutions (color) at 5 K and simulations (black). Simulated spin Hamiltonian parameters are given in Table S4.

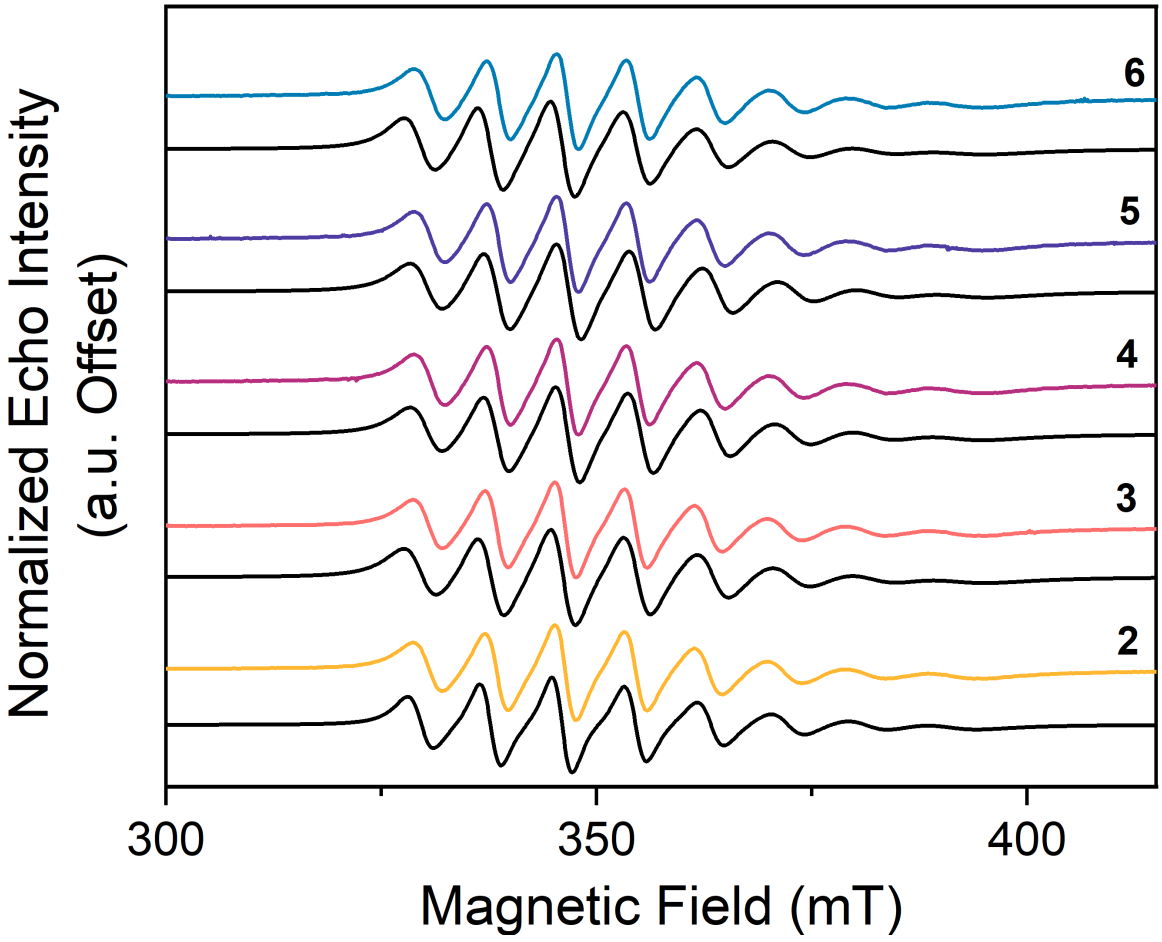

Figure S18. Continuous wave spectra at 9.4 GHz of **1**–**6** in toluene solutions (color) at 298 K and simulations (black). Simulated spin Hamiltonian parameters are given in Table S5.

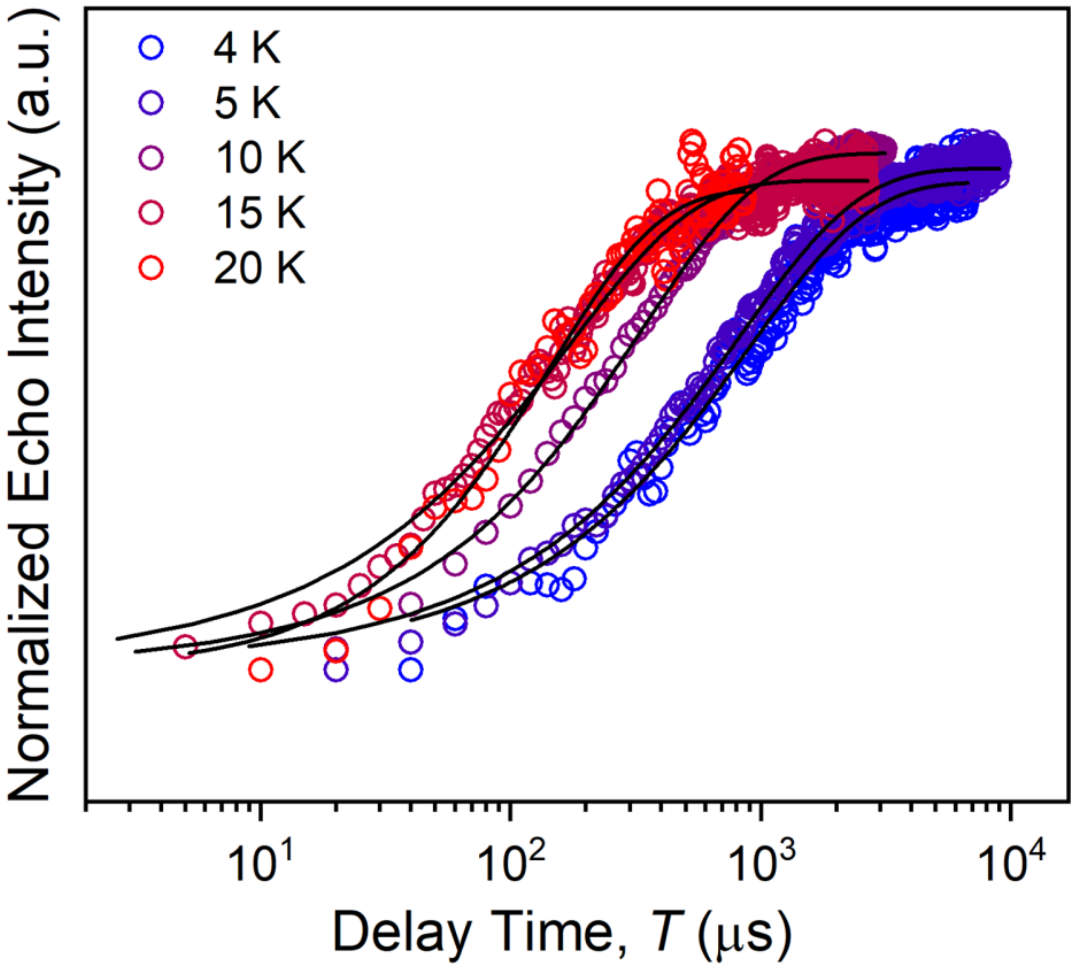

Figure S19. Selected variable temperature inversion recovery curves (color traces) and fits (black traces) for **1** in d^{14}-*o*-terphenyl.

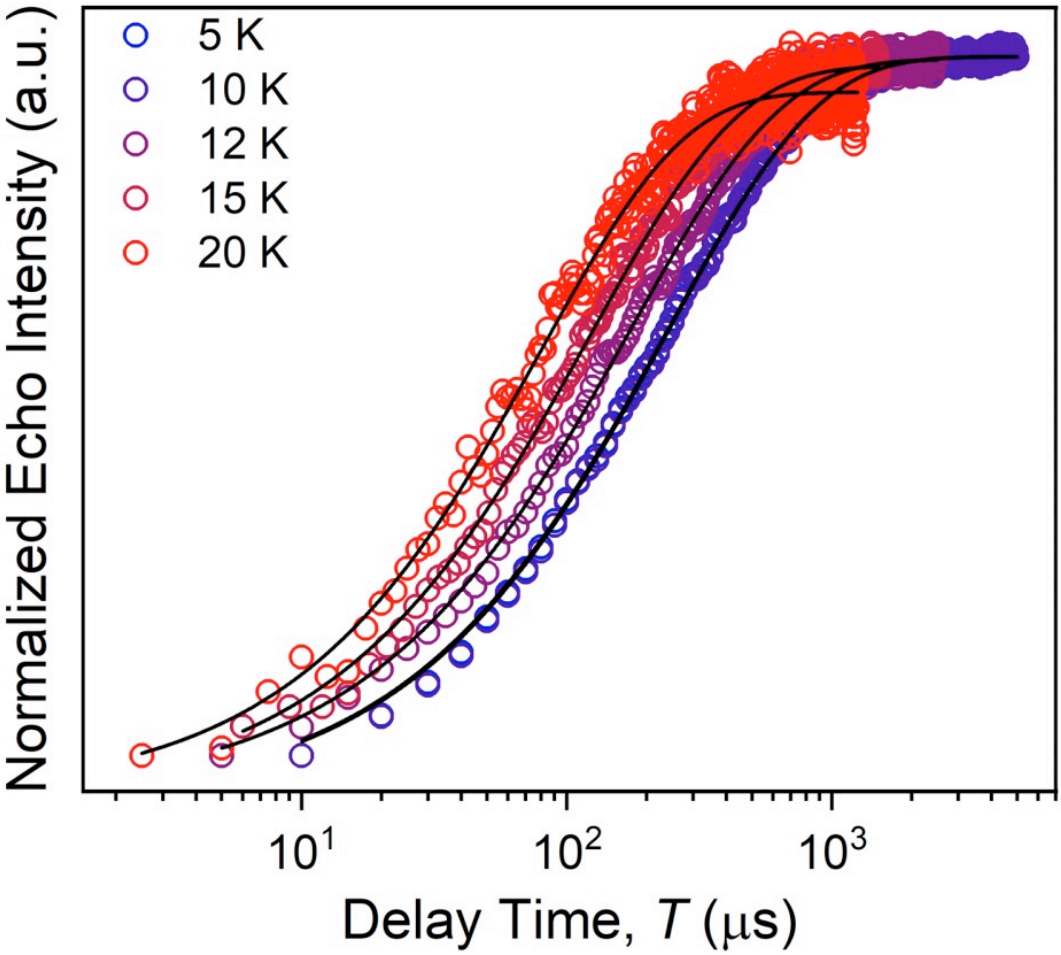

Figure S20. Selected variable temperature inversion recovery curves (color traces) and fits (black traces) for **2** in d^{14}-*o*-terphenyl.

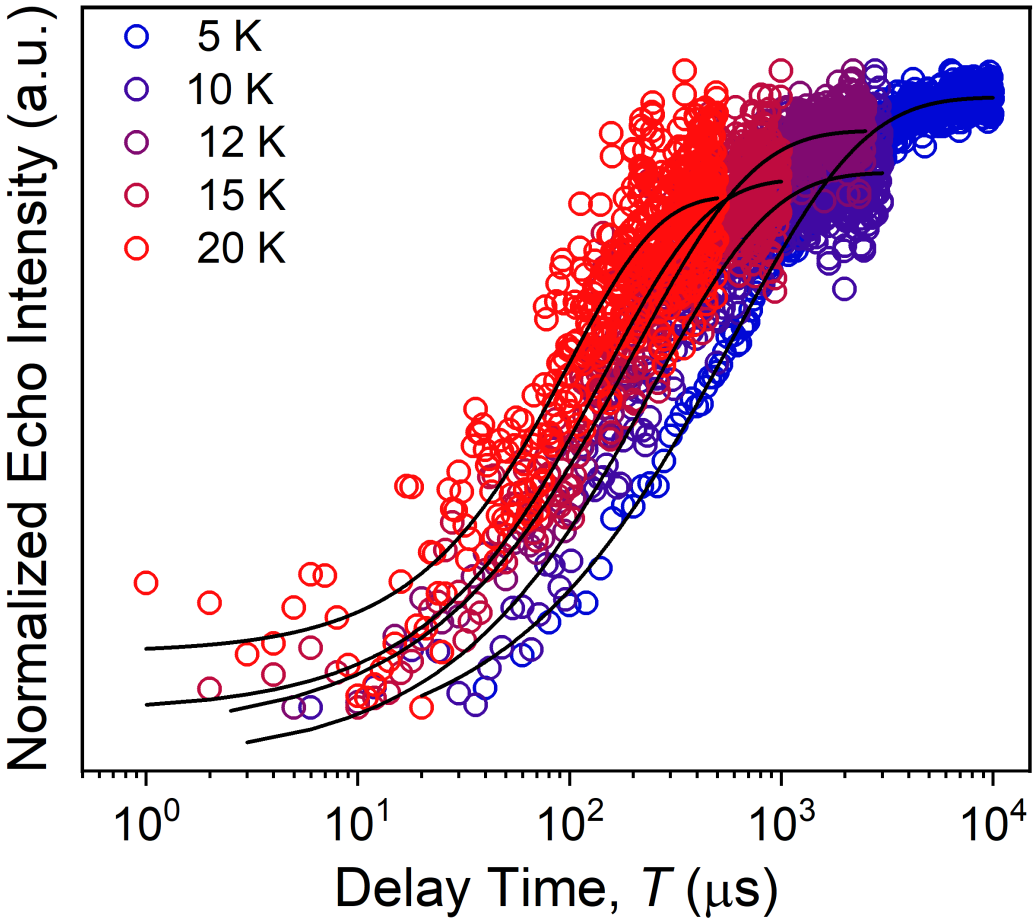

Figure S21. Selected variable temperature inversion recovery curves (color traces) and fits (black traces) for **3** in d^{14}-*o*-terphenyl.

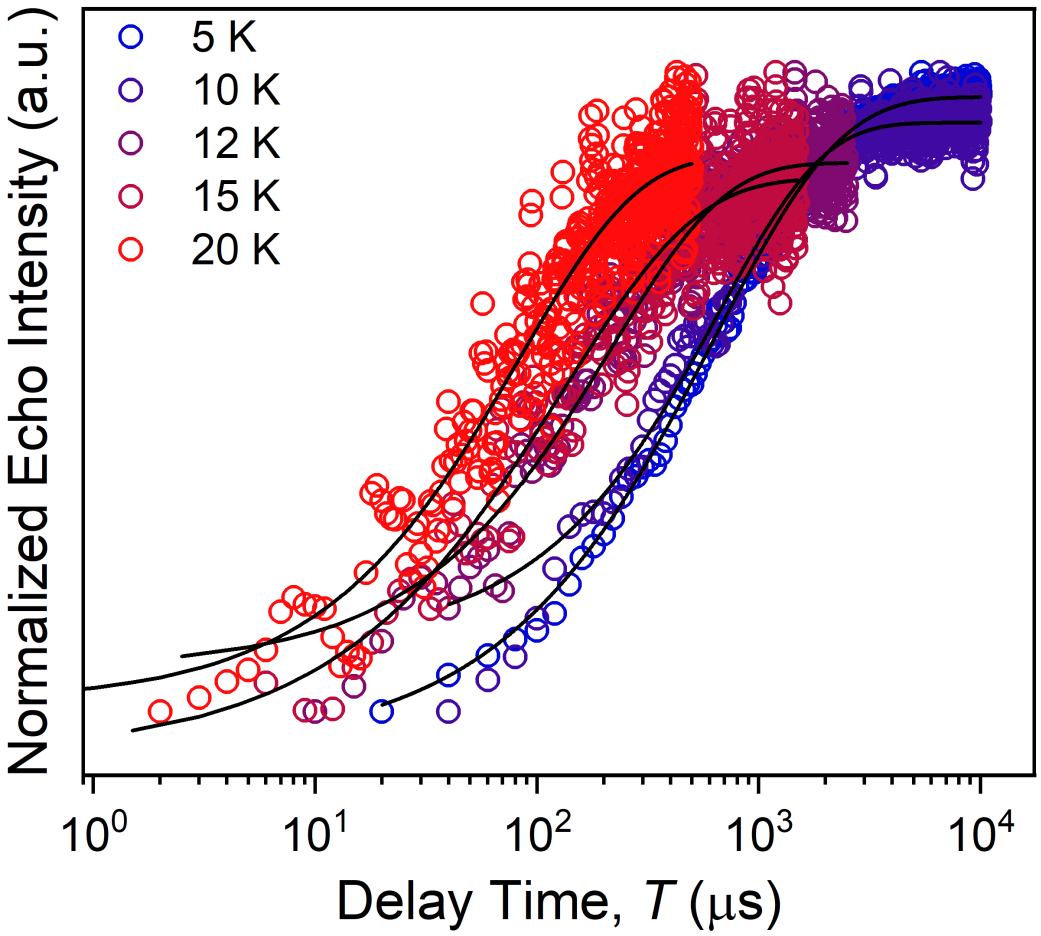

Figure S22. Selected variable temperature inversion recovery curves (color traces) and fits (black traces) for **4**.

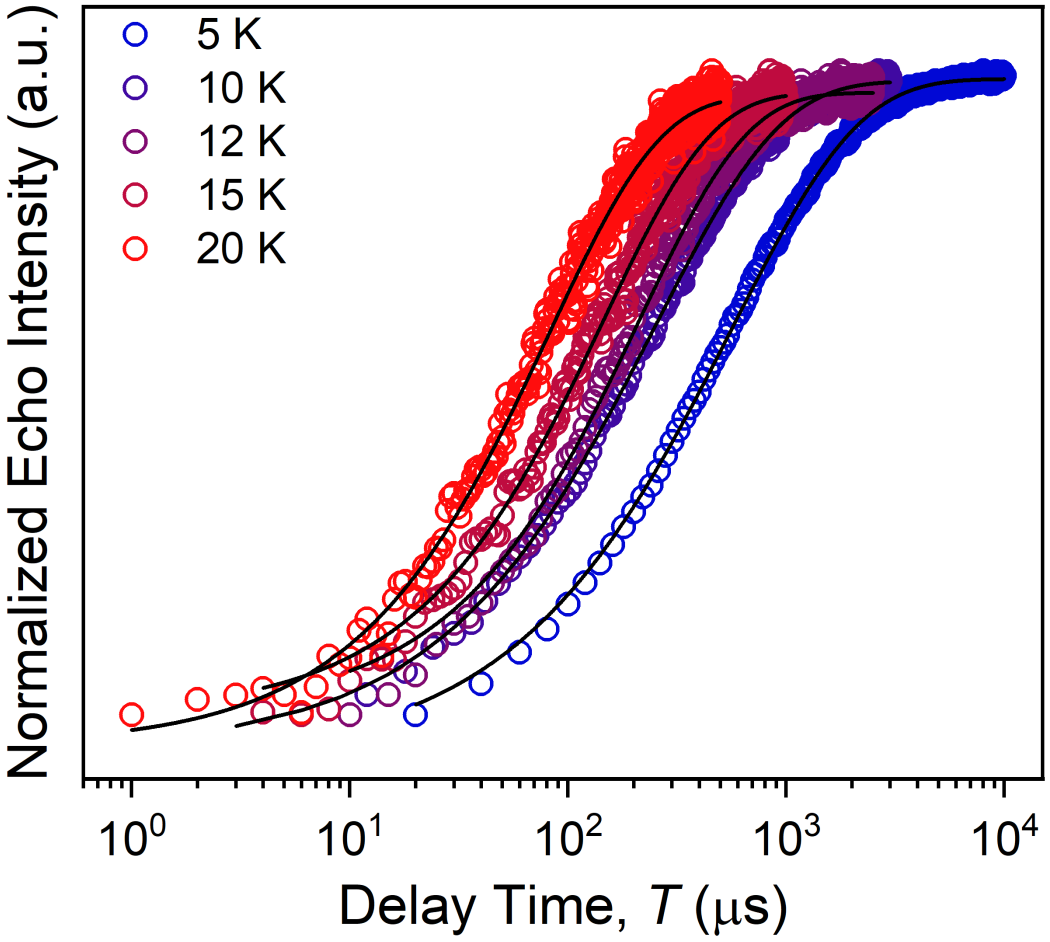

Figure S23. Selected variable temperature inversion recovery curves (color traces) and fits (black traces) for **5** in d^{14}-*o*-terphenyl.

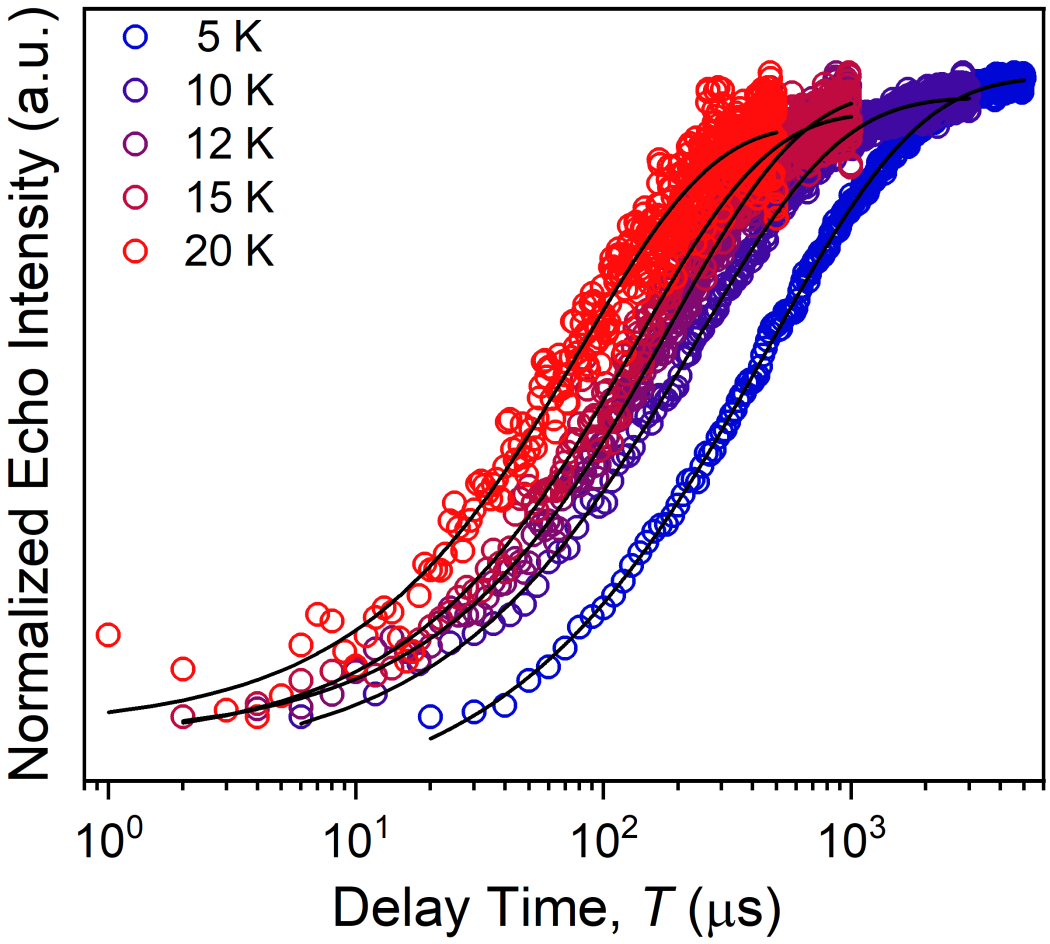

Figure S24. Selected variable temperature inversion recovery curves (color traces) and fits (black traces) for **6** in d^{14}-*o*-terphenyl.

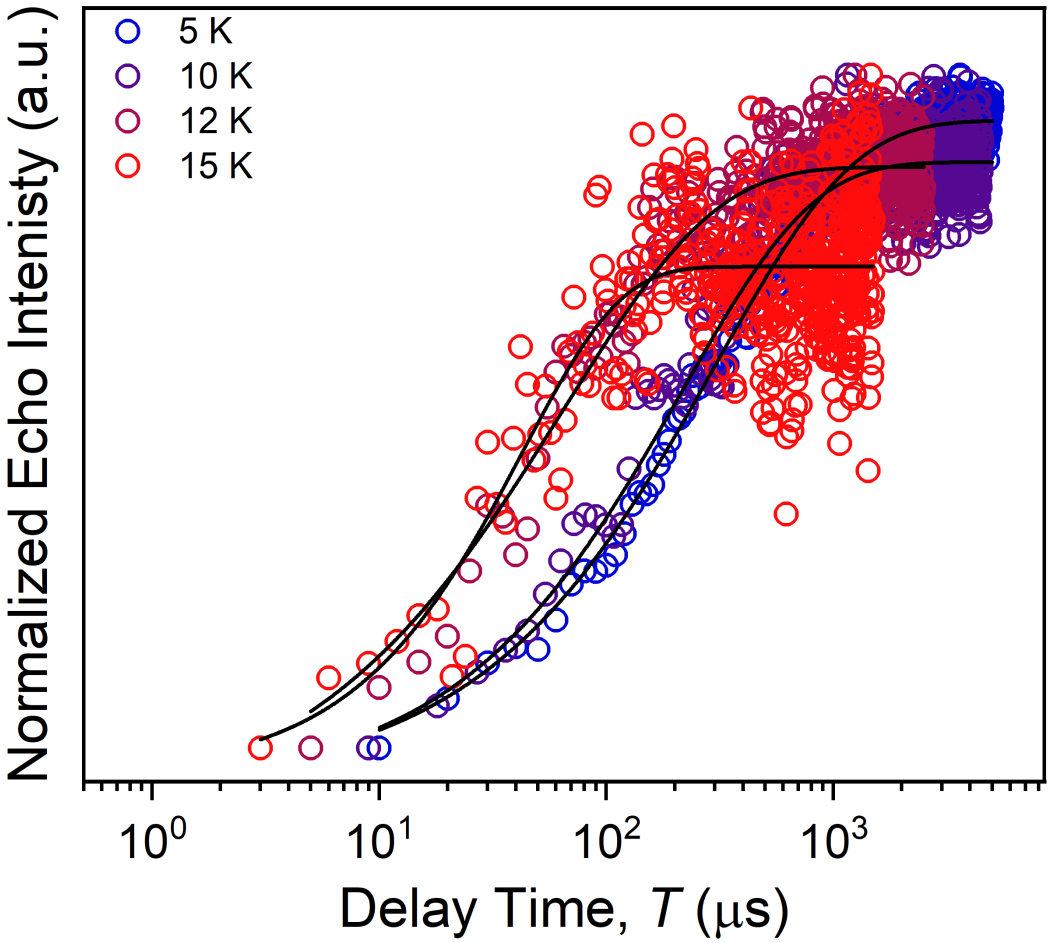

Figure S25. Selected variable temperature inversion recovery (color traces) and fits (black traces) for **7** in d^{14}-*o*-terphenyl.

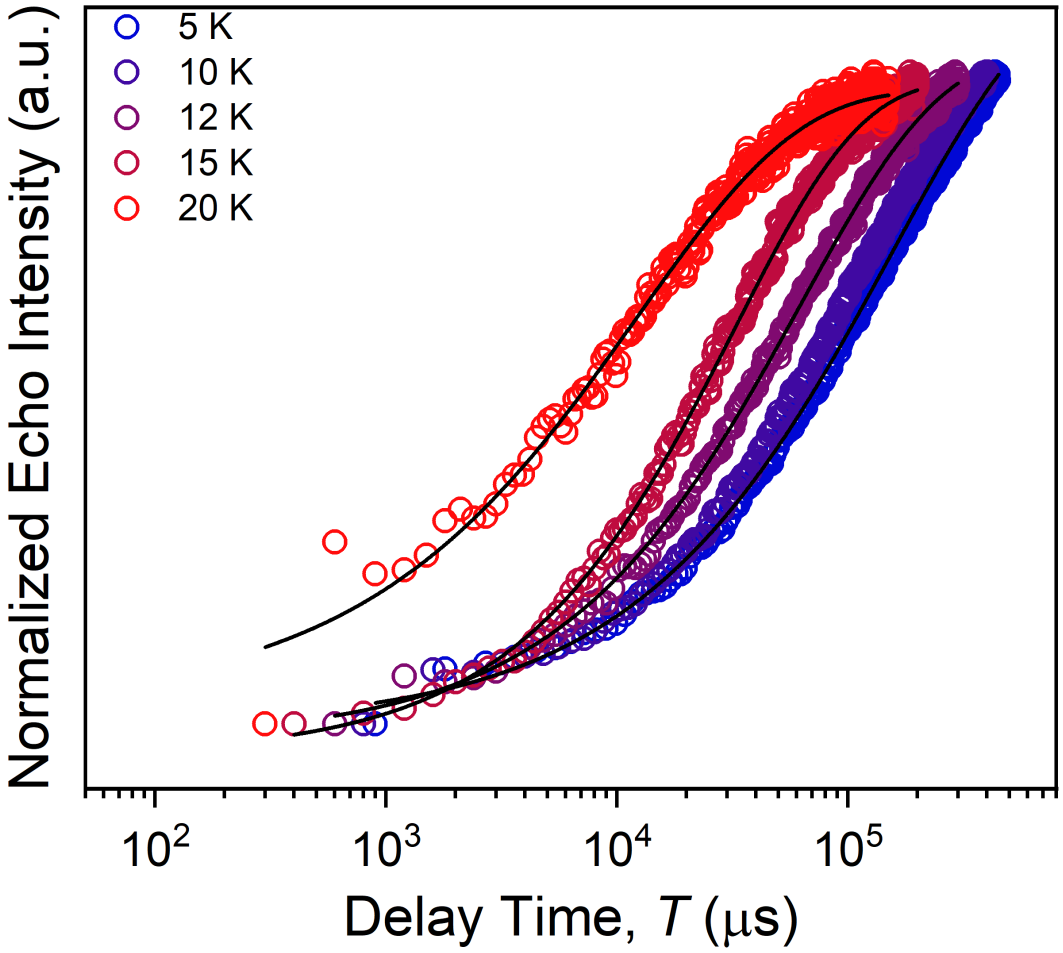

Figure S26. Selected variable temperature inversion recovery (color traces) and fits (black traces) for **8** in d^{14}-*o*-terphenyl.

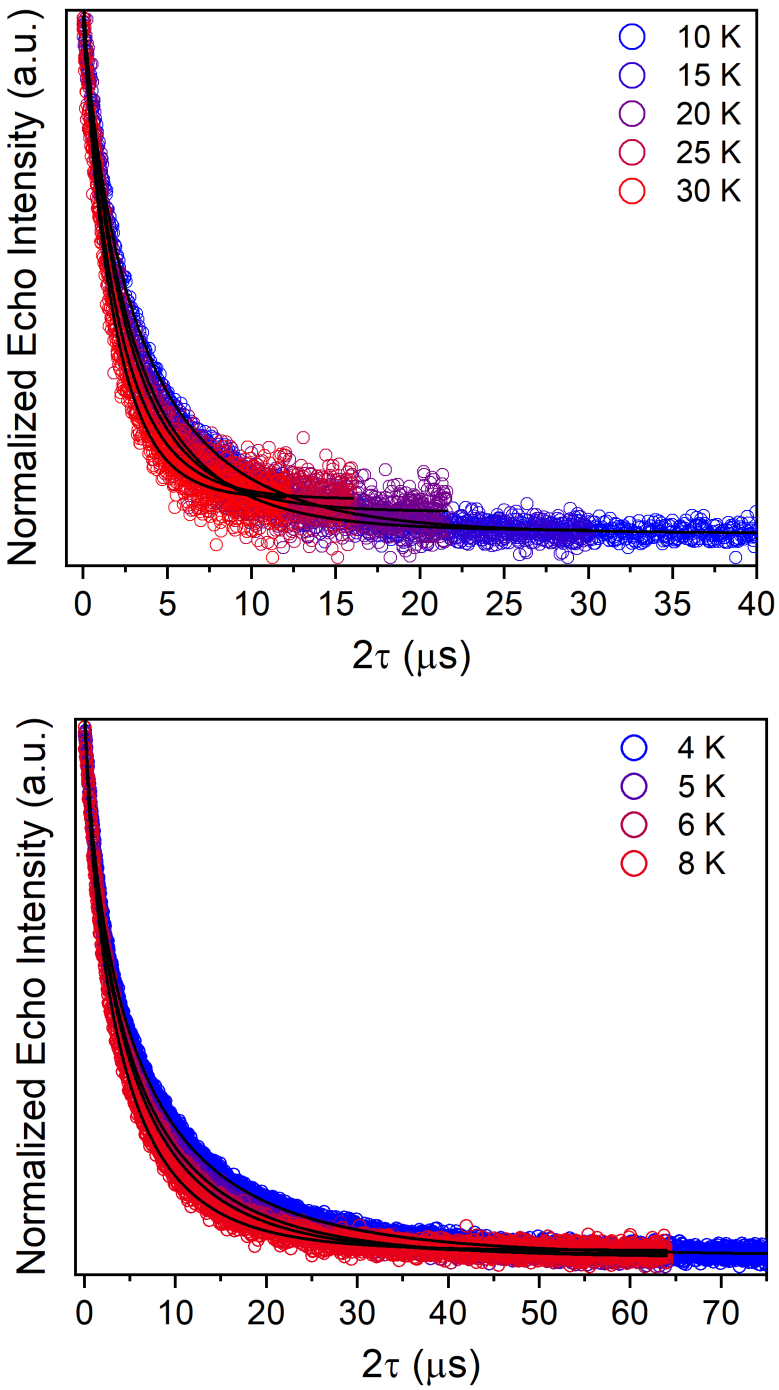

Figure S27. Selected variable temperature Hahn echo decay curve (color traces) and fits (black traces) for **1** in d^{14}-*o*-terphenyl at 120 GHz.

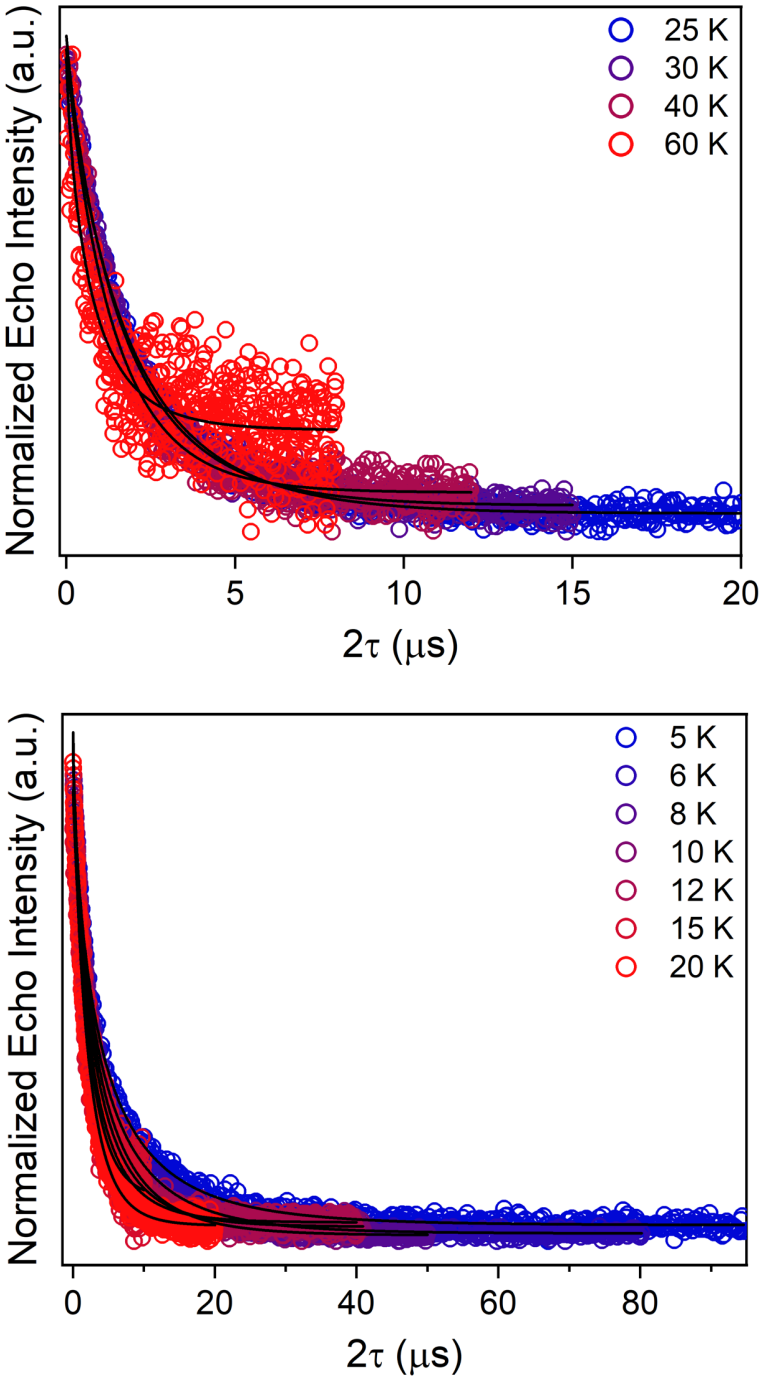

Figure S28. Selected variable temperature Hahn echo decay curve (color traces) and fits (black traces) for **2** in d^{14}-*o*-terphenyl at 120 GHz.

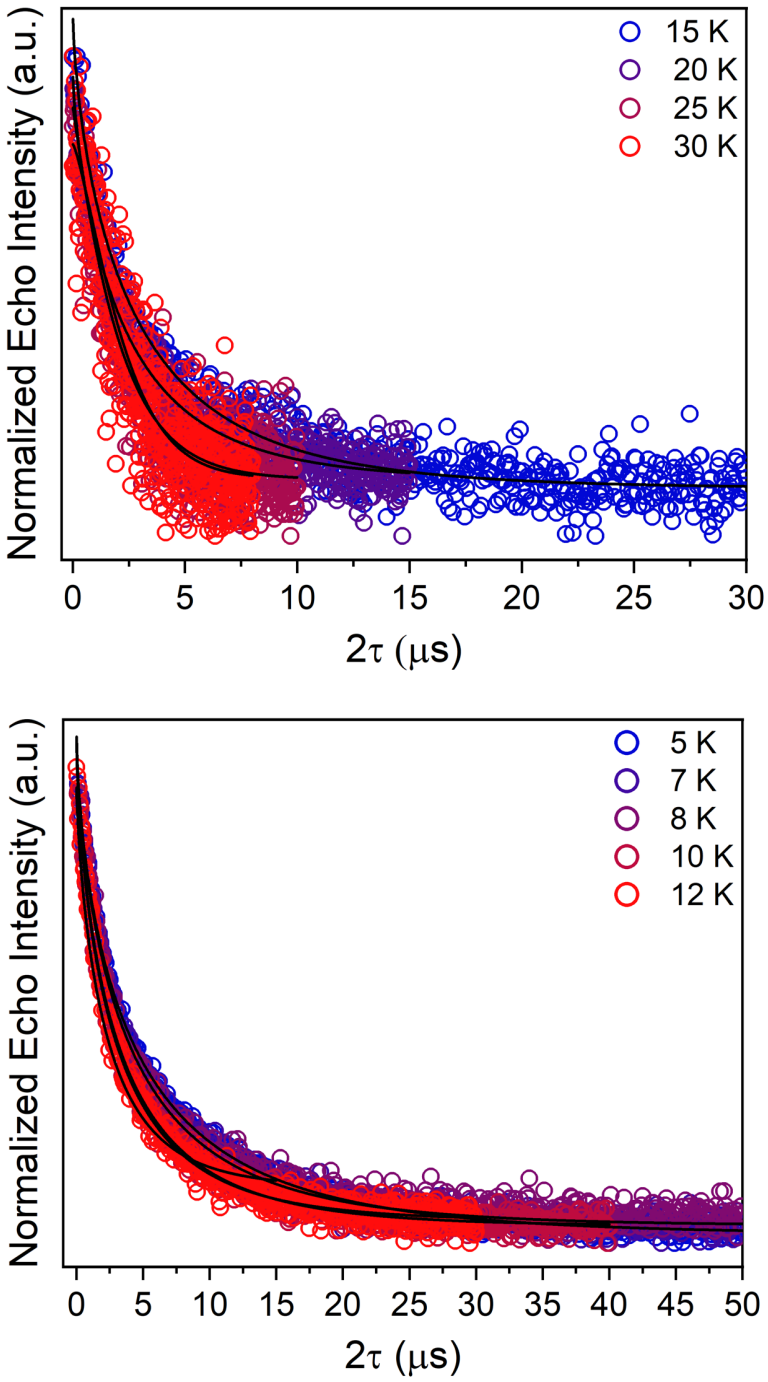

Figure S29. Selected variable temperature Hahn echo decay curve (color traces) and fits (black traces) for **3** in d^{14}-*o*-terphenyl at 120 GHz.

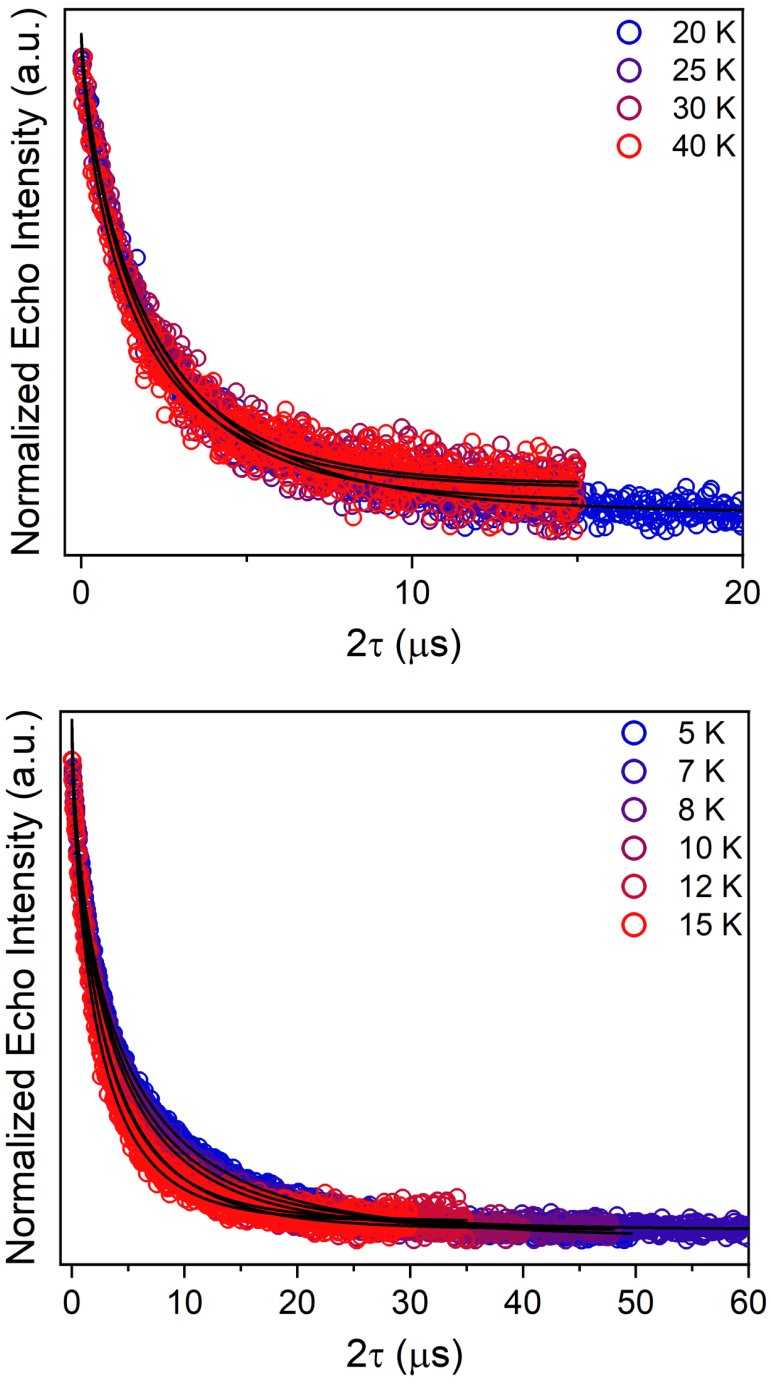

Figure S30. Selected variable temperature Hahn echo decay curve (color traces) and fits (black traces) for **4** in d^{14}-*o*-terphenyl at 120 GHz.

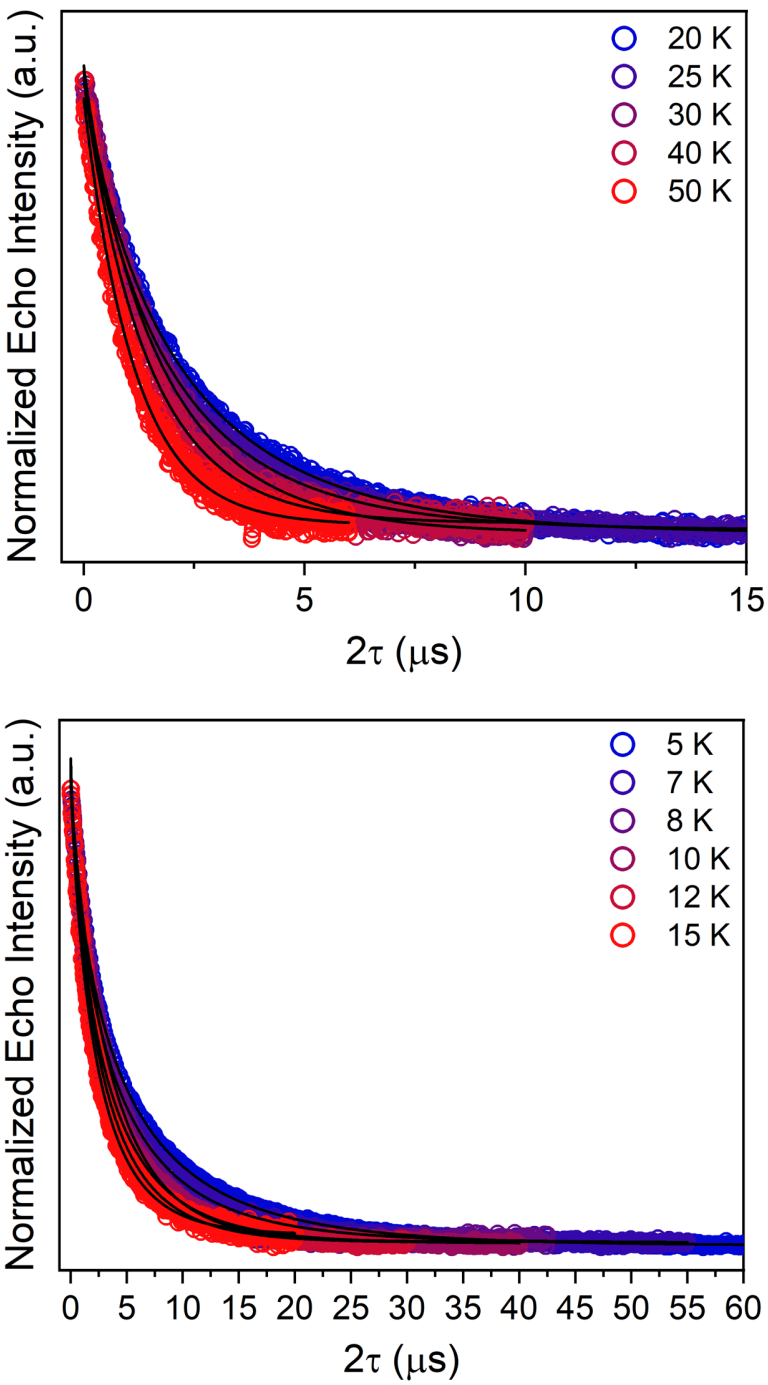

Figure S31. Selected variable temperature Hahn echo decay curve (color traces) and fits (black traces) for **5** in d^{14}-*o*-terphenyl at 120 GHz.

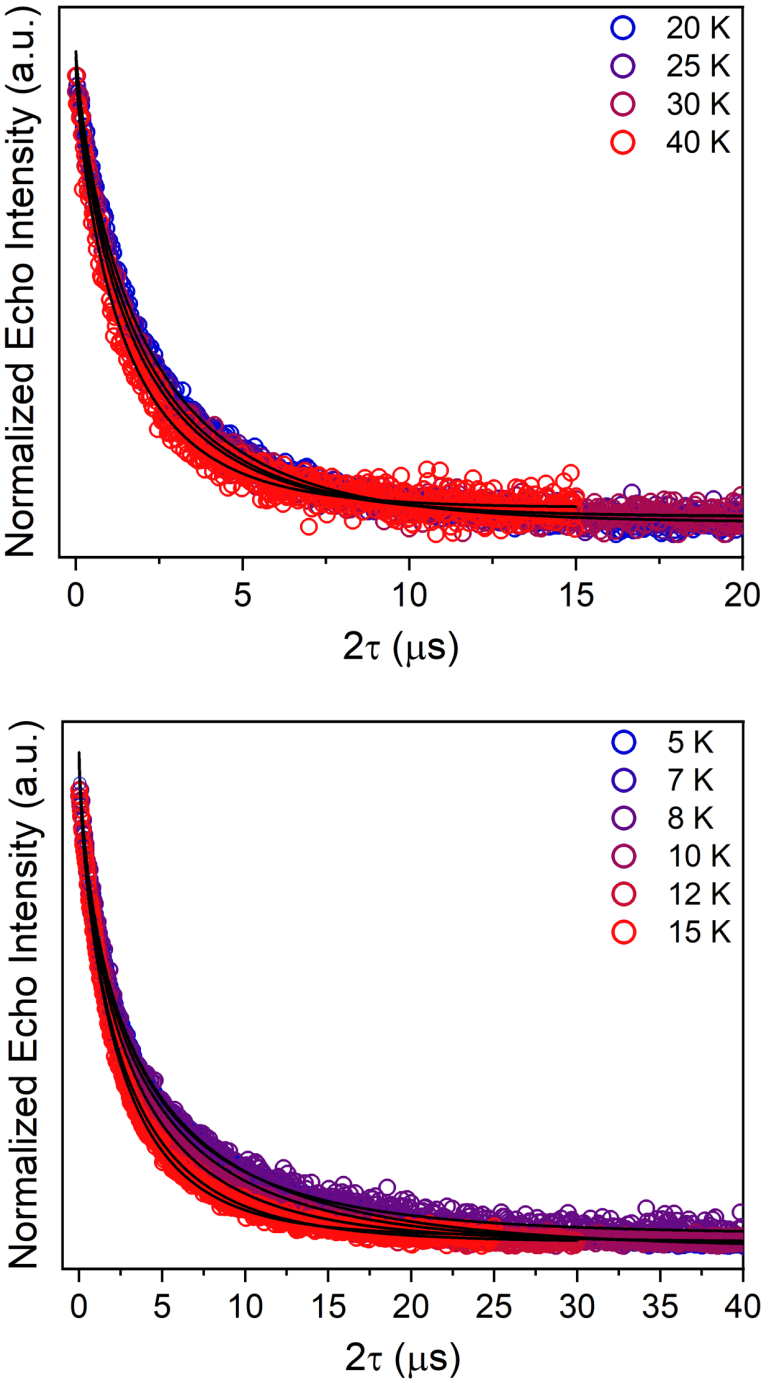

Figure S32. Selected variable temperature Hahn echo decay curve (color traces) and fits (black traces) for **6** in d^{14}-*o*-terphenyl at 120 GHz.

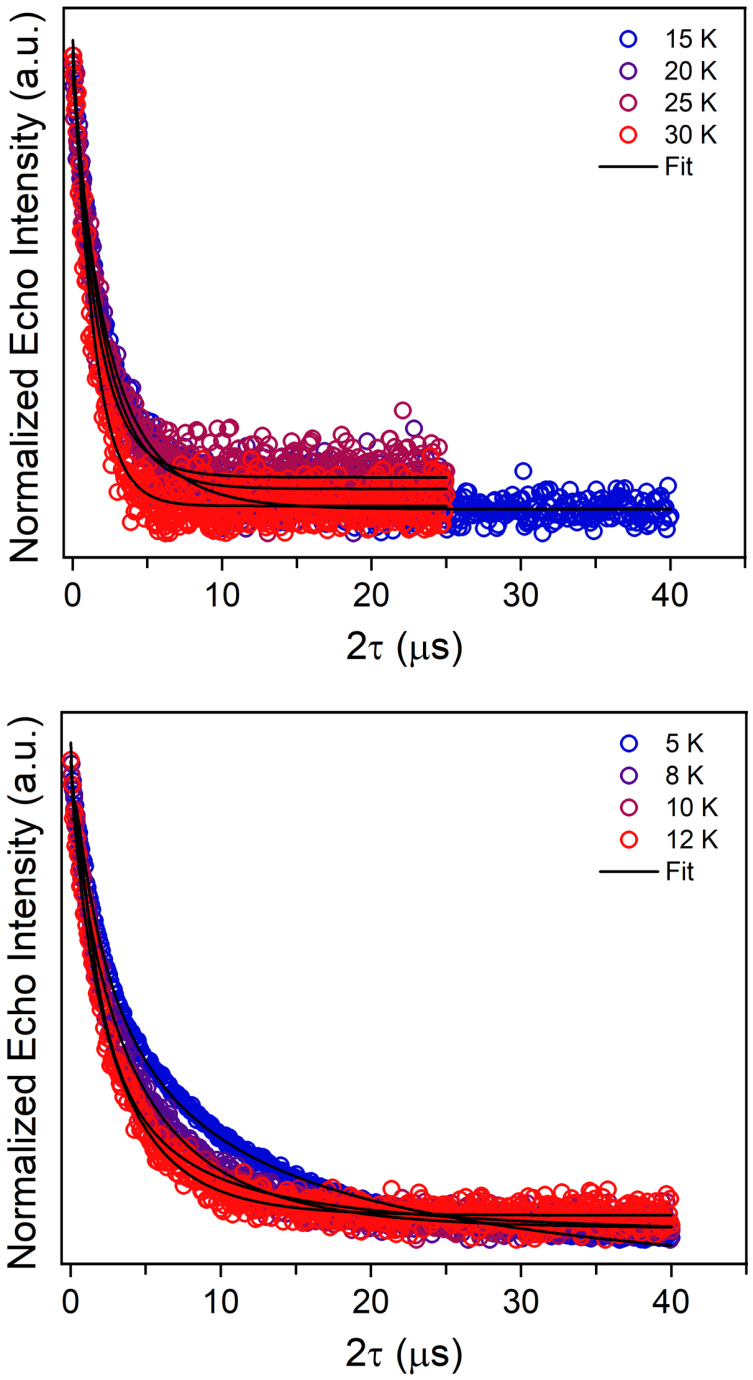

Figure S33. Selected variable temperature Hahn echo decay curve (color traces) and fits (black traces) for **7** in d^{14}-*o*-terphenyl at 120 GHz.

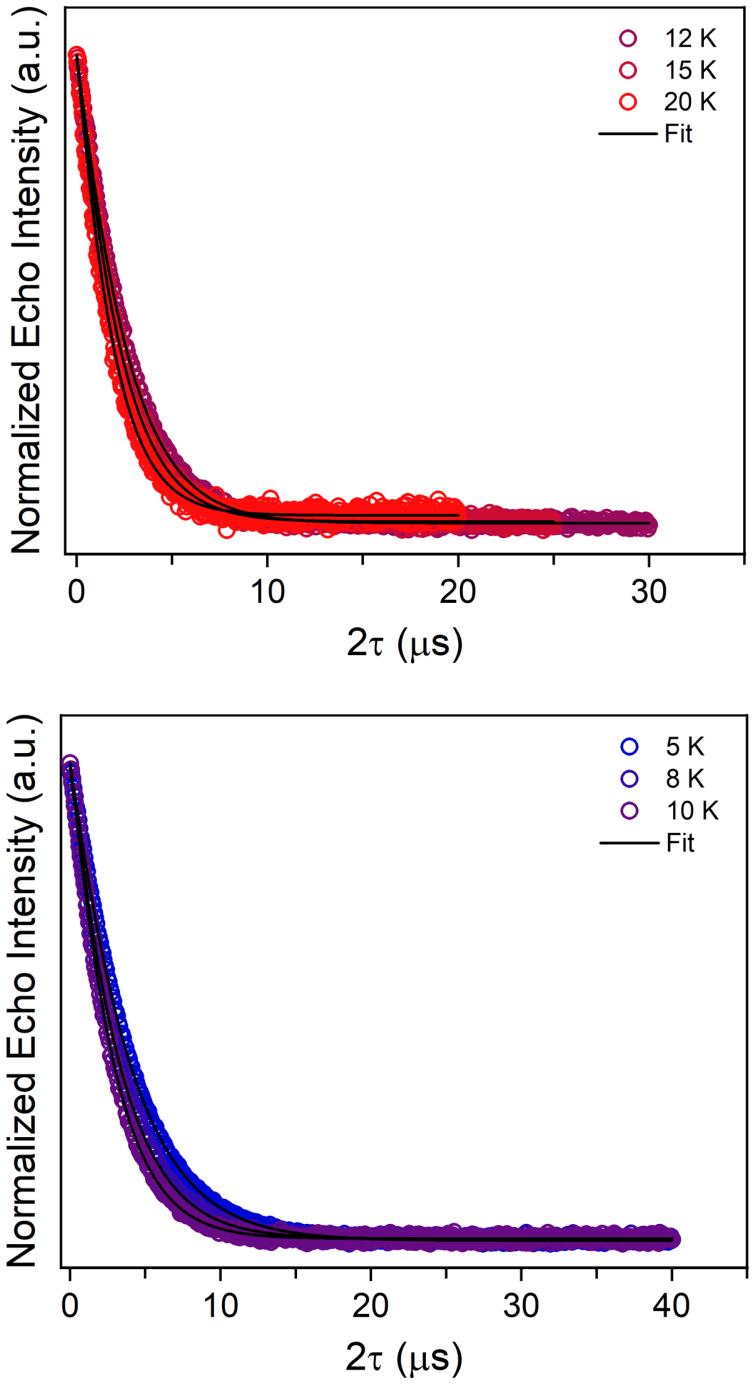

Figure S34. Selected variable temperature Hahn echo decay curve (color traces) and fits (black traces) for **8** in d^{14}-*o*-terphenyl at 120 GHz.

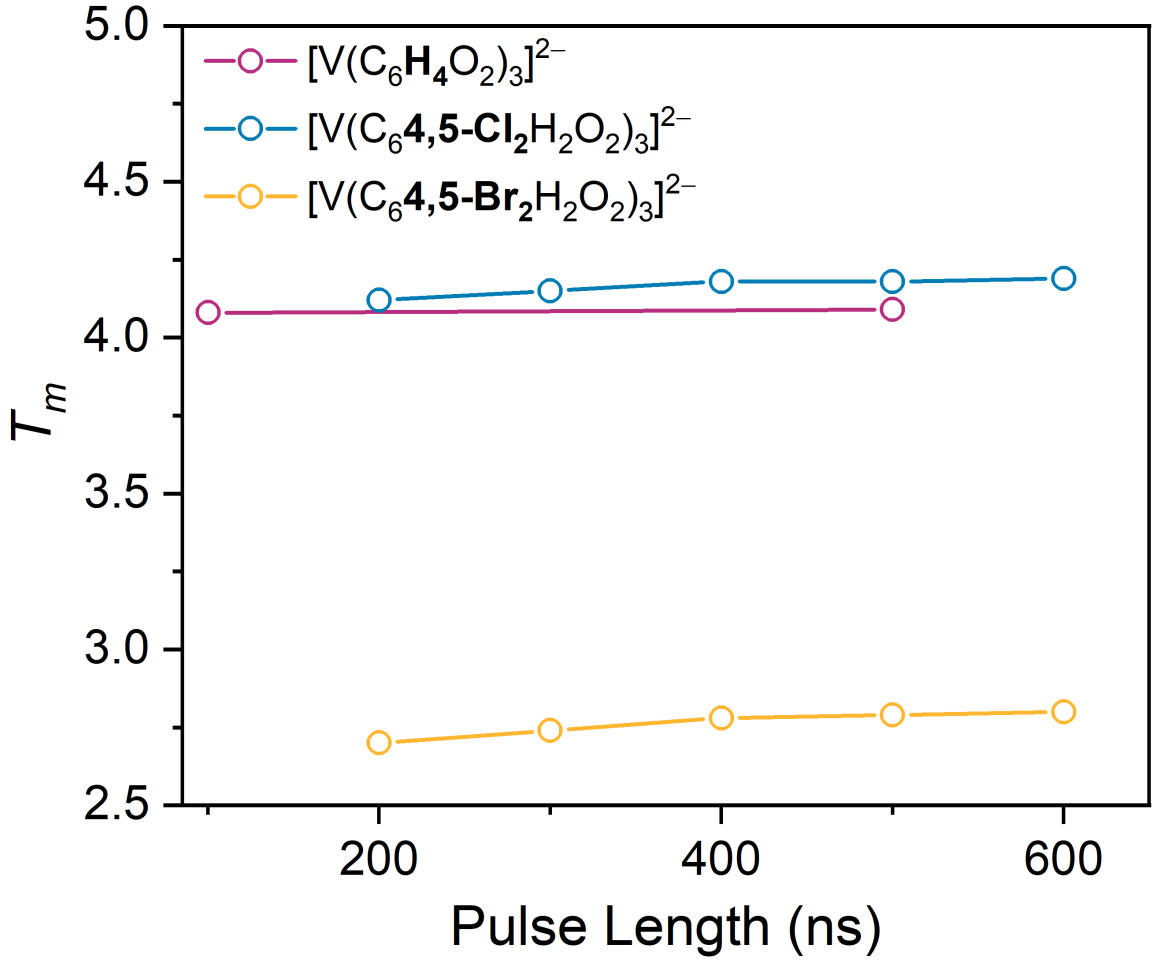

Figure S35. Comparison of instantaneous diffusion results of **1**, **5**, and the bromine analogue of **5** in d^{14}-*o*-terphenyl at 120 GHz.